

Learning Temporal Quantum Tomography

Quoc Hoan Tran^{1,*} and Kohei Nakajima^{1,2,†}

¹*Graduate School of Information Science and Technology,
The University of Tokyo, Tokyo 113-8656, Japan*

²*Next Generation Artificial Intelligence Research Center,
The University of Tokyo, Tokyo 113-8656, Japan*

(Dated: December 24, 2024)

Quantifying and verifying the control level in preparing a quantum state are central challenges in building quantum devices. The quantum state is characterized from experimental measurements, using a procedure known as tomography, which requires a vast number of resources. However, tomography for a quantum device with temporal processing, which is fundamentally different from standard tomography, has not been formulated. We develop a practical and approximate tomography method using a recurrent machine learning framework for this intriguing situation. The method is based on repeated quantum interactions between a system called quantum reservoir with a stream of quantum states. Measurement data from the reservoir are connected to a linear readout to train a recurrent relation between quantum channels applied to the input stream. We demonstrate our algorithms for representative quantum learning tasks, followed by the proposal of a quantum memory capacity to evaluate the temporal processing ability of near-term quantum devices.

Introduction.— The impressive progress in realizing quantum-enhanced technologies places a demand on the characterization and validation of quantum hardware. One of the most quintessential parts of building quantum devices is quantum process tomography (QPT), which is used in verifying quantum devices via the reconstruction of an unknown quantum channel from measurement data [1, 2]. Standard QPT approaches, which have been focused recently on small system size [3–7], assume the quantum device processes input states separately in a time-independent manner. In the envisioned picture of quantum time-series processing, the quantum device may output the states in a sequence where the current output depends on the past inputs and outputs. For example, the quantum device may generate temporal and input-dependent noise or fluctuations, which may have effects on the output states [8, 9]. Moreover, optical quantum states defined in temporal modes can be manipulated in a time-dependent and input-dependent manner using nonlinear optical processes [10, 11]. Performing tomography for such devices differs from standard QPT because of the higher dimensionality considering the time dimension.

Given a sequence of input quantum states β_1, β_2, \dots in a D_A -dimensional Hilbert space, a quantum device processes this sequence via a temporal map \mathcal{F} to output quantum states $\mathcal{F}(\beta_1), \mathcal{F}(\beta_2), \dots$ in a D_B -dimensional Hilbert space. Here, we take $D_A = D_B = D$ for notational simplicity. We assume that $\mathcal{F}(\beta_n)$ may depend on $\mathcal{F}(\beta_{n-1})$ and a finite number of past inputs. An intriguing example is the temporal depolarizing channel $\mathcal{F}(\beta_n) = p_n \frac{I}{D} + (1-p_n)\beta_n$, which replaces β_n with a completely mixed state I/D with probability p_n and leaves the state untouched otherwise. The dependency assumption can be established if p_n depends on p_{n-1}, p_{n-2}, \dots and $\beta_n, \beta_{n-1}, \dots$. Another example is the reproduction of previous states, where $\mathcal{F}(\beta_n) = \beta_{n-d}$ with a delay $d \geq 0$.

Generally, we consider a stream of unknown quantum channels $\Omega_1, \Omega_2, \dots$ applied to the input stream where there is a dependency between these channels [Fig. 1(a)]. The output $\mathcal{F}(\beta_n)$ can be considered as a mixed state of a finite number of the current and past channel's outputs

$$\mathcal{F}(\beta_n) = \frac{1}{Z} \sum_{i=0}^d \eta_i \Omega_{n-i}(\beta_{n-i}). \quad (1)$$

Here, η_i are unknown non-negative real numbers with $Z = \sum_{i=0}^d \eta_i$ to preserve the trace. This concept envisions a typical case in the future realization of quantum communication and quantum internet [12–14] where quantum data can be transmitted via time-dependent quantum channels under a time-delayed effect.

In this Letter, we propose a supervised learning framework to perform the approximate tomography of \mathcal{F} . A naive approach is to perform state tomography of $\mathcal{F}(\beta_n)$ for every n . This requires many repetition experiments on copies of $\mathcal{F}(\beta_n)$ and the inversion of a huge linear system to get a fixed tomography precision for every n [15]. Our idea is to simplify the experimental protocol and reduce the implementation cost under the assumption of the dependency in \mathcal{F} . We assume that it is possible to perform state tomography at some time steps as $\mathcal{F}(\beta_1), \dots, \mathcal{F}(\beta_L)$. We setup a learnable framework and train the recurrent relation in it to reconstruct $\mathcal{F}(\beta_n)$. Our framework considers a quantum system \mathcal{S} , called a *quantum reservoir* (QR), interacting with the input stream belonging to an auxiliary system \mathcal{E} . Each β_n interacts for a certain time with \mathcal{S} before being replaced by another one. The information of input states is sequentially transferred from \mathcal{E} into \mathcal{S} with a recurrent relation. The results of measurements in \mathcal{S} can be used as high-dimensional quantum features to train a regression model to output the density matrices that approximate $\mathcal{F}(\beta_1), \dots, \mathcal{F}(\beta_L)$ [Fig. 1(b)]. After this procedure, we

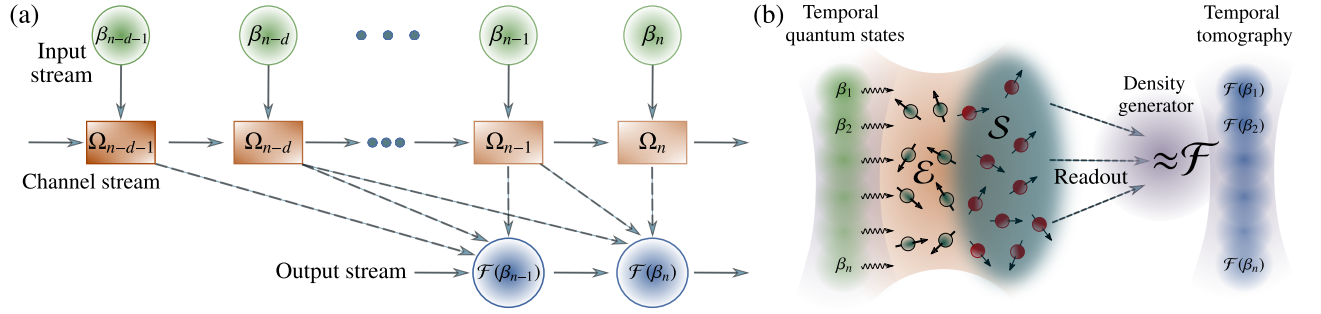


FIG. 1. Our framework can learn the tomography of a device that is supposed to implement an unknown temporal quantum map \mathcal{F} , or emulate a predefined \mathcal{F} . (a) A stream of quantum channels applies to the input stream where there is a dependency between channels (described by solid-line arrows). The device’s output at each time is a mixed state of a finite number of the current and past channel’s outputs. (b) Our framework consists of a quantum reservoir \mathcal{S} interacting with the input stream. The inputs are processed by some cycles of the time evolution, each cycle is followed by the measurement of \mathcal{S} . These measurement results are used in a readout layer to reconstruct \mathcal{F} .

are able to reconstruct $\mathcal{F}(\beta_n)$ for $n > L$ from the trained parameters by performing a single protocol of measurements in \mathcal{S} . The framework is applicable for different types of \mathcal{F} without reconfiguring the experimental bases.

Our framework is a quantum extension of classical reservoir computing (RC) to perform quantum tasks (Section I.A-B in [15]). The crucial principle of RC is to represent the input sequence by feeding the input into a dynamical system, called the reservoir, to encode all relevant nonlinear dynamics in high-dimensional trajectories [16–19]. Our proposal exploits quantum dynamics as a reservoir in the time-series processing of quantum data. This idea develops the initial proposal of harnessing disordered quantum dynamics for machine learning with classical time-series data [20–22]. While the RC approaches in tomography tasks focused on a static quantum state [23–25], our approach can process time-dependent quantum states. We further propose the concept of quantum memory capacity to uncover the temporal processing ability of near-term quantum devices.

Model. — Assume that the initial state of the coupled system (\mathcal{S}, \mathcal{E}) is a product state $\rho = \rho \otimes \beta$, where ρ and β are the state of \mathcal{S} and the reference state of \mathcal{E} , respectively. The coupled system is evolved under a unitary evolution U and the state ρ of \mathcal{S} is transformed via the *reduced dynamics map* \mathcal{L}_β , where $\mathcal{L}_\beta(\rho) = \text{Tr}_\mathcal{E}[U(\rho \otimes \beta)U^\dagger]$. Here, \mathcal{L}_β is a completely positive and trace-preserving map. The successive interactions are described as

$$\rho_n = \mathcal{L}_{\beta_n}(\rho_{n-1}) = \text{Tr}_\mathcal{E}[U(\rho_{n-1} \otimes \beta_n)U^\dagger], \quad (2)$$

where ρ_n is the state of \mathcal{S} for the n th interaction. We measure local observables O_1, \dots, O_K on ρ_n to obtain a high-dimensional feature vector called *reservoir state* \mathbf{x}_n . The k th element in \mathbf{x}_n can be calculated as $x_{nk} = \text{Tr}[O_k \rho_n] = \langle O_k \rangle_{\rho_n}$, which is the expectation of the measurement result via O_k . One can increase the dimension of \mathbf{x}_n by performing measurements at multiple times. Between two inputs, M cycles of the unitary evolution are

processed and each of them is followed by a measurement. M is called the measurement multiplexity, thus we obtain MK elements in each reservoir state.

In the training stage, we are given an input sequence $\{\beta_1, \dots, \beta_L\}$ and the target sequence $\{\hat{\mathbf{y}}_1, \dots, \hat{\mathbf{y}}_L\}$ where $\hat{\mathbf{y}}_k$ is the real vector form to stack the real and imaginary elements of $\mathcal{F}(\beta_k)$. Our framework includes a readout map h , which is simply taken as a linear combination of the reservoir states as $\mathbf{y}_n = h(\mathbf{x}_n) = \mathbf{w}^\top \mathbf{x}_n$. Here, \mathbf{w} is the parameter to be optimized by minimizing the mean-square error between \mathbf{y}_n and $\hat{\mathbf{y}}_n$ over $n = 1, \dots, L$. In the evaluation stage, we are given an input sequence $\{\beta_{L+1}, \dots, \beta_{L+T}\}$ with the target $\{\hat{\sigma}_{L+1}, \dots, \hat{\sigma}_{L+T}\}$ where $\hat{\sigma}_i = \mathcal{F}(\beta_i)$. The reconstructed output sequence is $\{\mathbf{y}_{L+1}, \dots, \mathbf{y}_{L+T}\}$, which is rearranged in the matrix form $\{\sigma_{L+1}, \dots, \sigma_{L+T}\}$ [26]. Since targets are density matrices, we use the fidelity $F(\rho, \sigma) = \left(\text{Tr}[\sqrt{\sqrt{\sigma}\rho\sqrt{\sigma}}]\right)^2$ to estimate the reconstruction error. In error-free tomography, $F = 1$, and $F < 1$ otherwise. We calculate the root mean square of fidelities in the evaluation stage as $\text{RMSF} = \sqrt{\frac{1}{T} \sum_{i=L+1}^{L+T} F^2(\hat{\sigma}_i, \sigma_i)}$.

The reservoir’s response to the same input sequence may differ with different initial states of the reservoir and may result in the loss of reproducibility in the temporal processing. In order to prevent this effect, the time evolution of the reservoir must mostly depend on the input sequence after enough transient time. This property is known as the echo state property [16] in classical RC or the quantum echo state property (QESP) in quantum RC [27, 28]. QESP ensures the fading memory property [29], which is the ability of the reservoir to retain information about recent inputs for proper learning of functions of the past inputs. Based on the spectrum of reduced dynamics maps, we can evaluate the QESP time scale, which indicates the transient time to forget the QR’s initial state before learning (Section II in [15]).

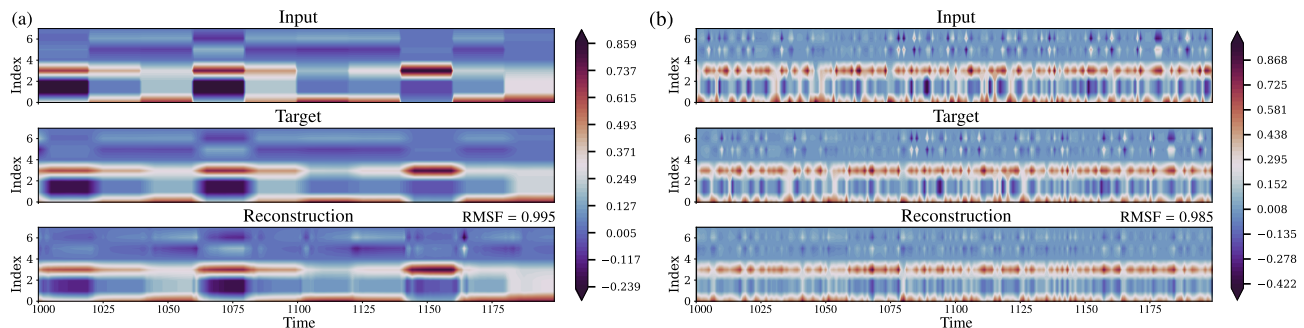


FIG. 2. Results of temporal tomography for (a) the quantum simple moving average filter and (b) the delayed depolarizing map with $d = 5$, $N_m = 5$, $N_e = 1$, $\alpha = 1.0$, $J = B = 1.0$, and $\tau B = 2.6$ (for (a)) and $\tau B = 2.0$ (for (b)). At each time point, the density matrix is represented as a 8-dimensional vector by stacking the real and imaginary parts, where the range of values is indicated in the color bars.

Results.—We present concrete applications of learning temporal tomography. We consider the coupled system $(\mathcal{S}, \mathcal{E})$ as a closed system of the transverse field Ising model with the unitary $U = \exp(-i\tau H)$, where the Hamiltonian $H = -\sum_{i>j=1}^N J_{i,j} \hat{s}_i^x \hat{s}_j^x - B \sum_j^N \hat{s}_j^z$ is unchanged during interaction time τ . Here, B is the natural frequency of 1/2-spins represented for qubits and \hat{s}_j^γ ($\gamma \in \{x, y, z\}$) are the Pauli operators measuring the qubit j along the γ direction. We present the setting of *power-law decaying* for $J_{ij} = J|i-j|^{-\alpha}/N(\alpha)$ with an interaction strength J , power coefficient α ($0 < \alpha < 3$), and $N(\alpha) = \sum_{i>j} |i-j|^{-\alpha}/(N-1)$ [30–32]. We assume that \mathcal{E} includes the first N_e spins where the remaining $N_m = N - N_e$ spins form the reservoir \mathcal{S} .

In our learning tasks, the number of observables is set to $K = N_m$ if we select observables as spin projections \hat{s}_j^z over the z -axis for all j , and to $K = N_m(N_m + 1)/2$ if we further select observables as two-spin correlations $\hat{s}_i^z \hat{s}_j^z$ for all $i < j$. We set Ω_n in Eq. (1) as the time-dependent depolarizing quantum channel $\Omega_n(\beta) = p_n \frac{I}{D} + (1 - p_n)\beta$. To introduce a temporal dependency between Ω_n , the depolarizing probability p_n is formulated as the r th-order nonlinear dynamical output [33]: $p_n = \kappa p_{n-1} + \eta p_{n-1} \left(\sum_{j=0}^{r-1} p_{n-j-1} \right) + \gamma u_{n-r+1} u_n + \delta$, where $r = 10$, $\kappa = 0.3$, $\eta = 0.04$, $\gamma = 1.5$, and $\delta = 0.1$. Here, $\{u_n\}$ is a random sequence of scalar values in $[0, 0.2]$ to set p_n into the stable range in $[0, 1]$.

We first consider \mathcal{F} as a quantum simple moving average filter $\mathcal{F}(\beta_n) = \frac{1}{d+1} \sum_{i=0}^d \Omega_{n-i}(\beta_{n-i})$ [Fig. 2(a)] or a delayed depolarizing map $\mathcal{F}(\beta_n) = \Omega_{n-d}(\beta_{n-d})$ [Fig. 2(b)]. These examples are interesting since the reservoir scheme must memorize both the previous input states and properties of previous quantum channels. We set the delay $d = 5$, the number of qubits $N_m = 5$, $N_e = 1$, and $K = N_m$ and $M = 5$. Other model parameters are $\alpha = 1.0$, $J = B = 1.0$, and the normalized time $\tau B = 2.6$ (for Fig. 2(a)) and $\tau B = 2.0$ (for Fig. 2(b)). The number of time steps used in the initial transients, training, and evaluation stages are 500, 500, and 200,

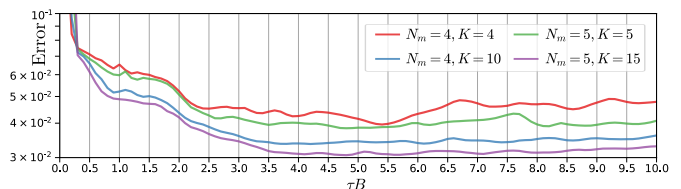


FIG. 3. Tomography errors according to τB for $\mathcal{F}(\beta_n) = \Omega_{n-1}(\beta_{n-1})$ with $\alpha = 1.0$ and $J = B = 1.0$.

respectively. At each time point, the density matrix is represented as a $2D^2$ -dimensional vector ($D = 2^{N_e}$) by stacking the real and imaginary parts. In Fig. 2(a), the input states jump to a new random quantum state every 20 time steps, thus introducing temporal dependencies between input states. Alternately, we consider a sequence of i.i.d. random input states in Fig. 2(b). The target sequences (middle panels in Fig. 2) in the evaluation stage can be almost perfectly reconstructed since the RMSF values in both cases are above 98% (bottom panels).

Next, we investigate the dependency of the task’s performance on the QR’s parameters. Figure 3 illustrates the tomography errors (1.0 - RMSF) according to τB in the reconstruction of $\mathcal{F}(\beta_n) = \Omega_{n-1}(\beta_{n-1})$ at $N_e = 2$ and $N_m = 4, 5$ qubits. The transients, training, and evaluation time steps are 1000, 3000, and 1000, respectively. The errors are averaged over 10 different runs with random trials of the input sequence and initial state. The errors reduce quickly at low values of τB and then settle to the stable lower values. We confirm that increasing N_m, M and K indeed scales the fidelity (see Fig. S11 in [15]). Table I presents the average errors along with their standard deviations at $\tau B = 10.0$ and $M = 5$. Particularly, with $N_m = 5$ and $K = 15$, the errors are lower than 1%, 4%, 6%, and 8% for $N_e = 1, 2, 3$, and 4 qubits, respectively. Furthermore, our method with the memory effect outperforms the classical baseline (last line in Table I) using linear regression (without a memory) to obtain outputs directly from input density matrices [34].

TABLE I. Average and standard deviation (mean \pm sd) of the tomography errors (%) for $\mathcal{F}(\beta_n) = \Omega_{n-1}(\beta_{n-1})$ of the baseline and our method at $\tau B = 10.0$ and $M = 5$.

| (N_m, K) | $N_e = 1$ | $N_e = 2$ | $N_e = 3$ | $N_e = 4$ |
|------------|---------------|---------------|----------------|----------------|
| (4, 4) | 0.9 \pm 0.0 | 4.8 \pm 0.1 | 8.0 \pm 0.0 | 8.9 \pm 0.1 |
| (5, 5) | 0.9 \pm 0.0 | 4.0 \pm 0.1 | 7.6 \pm 0.0 | 8.6 \pm 0.1 |
| (4, 10) | 0.9 \pm 0.0 | 3.6 \pm 0.1 | 6.4 \pm 0.0 | 8.3 \pm 0.1 |
| (5, 15) | 0.9 \pm 0.0 | 3.3 \pm 0.0 | 5.6 \pm 0.0 | 7.7 \pm 0.0 |
| Baseline | 3.2 \pm 0.1 | 9.2 \pm 0.1 | 10.0 \pm 0.1 | 10.2 \pm 0.1 |

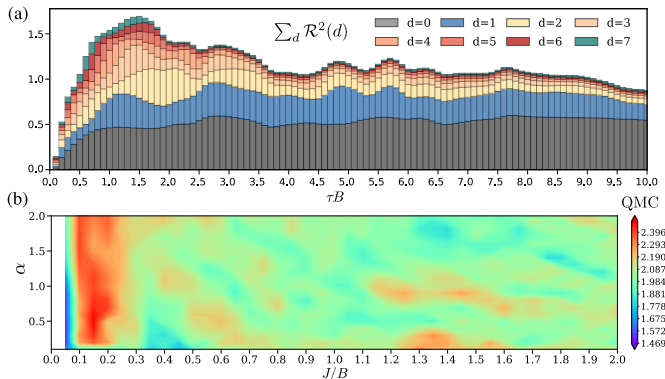


FIG. 4. (a) QMC broken down in delays d according to τB with $N_e = 2$, $N_m = 4$ with $\alpha = 1.0$ and $J = B = 1.0$. (b) The color map of QMC as the function of α and J/B at $\tau B = 10.0$.

We further investigate the *short-term memory* (STM) of the QR via the delay-reconstruction task $\mathcal{F}(\beta_n) = \beta_{n-d}$. The STM in the classical context is defined via the coefficient of determination to measure how much variance of the delay inputs can be recovered from outputs [35]. Since the input and output of our framework are density matrices, we define the d -delay STM of the QR by the squared distance correlation [36] between the output $\{\sigma_n\}$ and the target $\{\hat{\sigma}_n\} = \{\beta_{n-d}\}$:

$$\mathcal{R}^2(d) = \frac{\mathcal{V}^2(\{\sigma_n\}, \{\hat{\sigma}_n\})}{\sqrt{\mathcal{V}^2(\{\sigma_n\}, \{\sigma_n\})\mathcal{V}^2(\{\hat{\sigma}_n\}, \{\hat{\sigma}_n\})}}. \quad (3)$$

Here, \mathcal{V}^2 represents the squared distance covariance of two random sequences of density matrices [15]. $\mathcal{R}^2(d)$ is between 0 and 1, and represents the fraction of distance variance explainable in the sequence of output states by the sequence of delayed input states. We then define the quantum memory capacity, $\text{QMC} = \sum_{d=0}^{\infty} \mathcal{R}^2(d)$, to measure how much distance variance of the delay input states can be recovered from output states, summed over all delays. Quantifying QMC provides insights into the memory and temporal processing capability of the QR before applying it to a specific task. Furthermore, QMC can generally be used as a standard quantity to compare the temporal processing capacity of quantum devices.

Figure 4(a) shows QMC as a function of τB broken down in values of d ($0 \leq d \leq 7$) with the model pa-

rameters $\alpha = 1$, $J = B = 1.0$, $K = N_m = 4$, $N_e = 2$, and $M = 1$ (see other results in Section IV in [15]). $\mathcal{R}^2(d)$ is averaged over different runs with 10 random trials of the initial state and input sequence. This value is faded out with an increase in the delay $d \geq 7$. The total $\sum_{d=0}^{d=7} \mathcal{R}^2(d)$ increases and obtains the peak value at the onset of the dynamical transition region ($1.5 < \tau B < 2.5$) of the reduced dynamics map \mathcal{L}_β (Fig. S2(a) in [15]). We further examine the relation between QMC and other model parameters in Fig. 4(b), which displays the average QMC (calculated until $d_{\max} = 10$) as the function of α and J/B at $\tau B = 10.0$. Interestingly, QMC achieves highest values in the region $0.1 < J/B < 0.2$, which is referred to the dynamical transition in Figs. S3 and S6 in [15]. These observations can be explained by the difference in the eigenvalues' distribution of \mathcal{L}_β (Figs. S2(a) and S3 in [15]). The regime with eigenvalues concentrated near the border of the unit disk leads toward a unitary behavior. Therefore, only a little information of the input state β is remained after applying \mathcal{L}_β , which is unfavorable on temporal learning tasks. In contrast, the regime with eigenvalues concentrated near the center of the unit disk guarantees enough information in the input states to be entangled with the QR. Here, the dynamics becomes ergodic and the local observables become functions of a finite number of past inputs. We anticipate that QMC builds up first as the dynamics moves from more unitary to more ergodic regime and obtains the peak at the transition between these regimes. For temporal classical tasks in quantum spin networks, similar observations [37] have also been investigated recently to address the impact of the transition between localization and thermalization manifest [38].

Conclusion and Discussion.— We formulate and propose the general framework for learning tomography of temporal quantum maps acting on quantum data. We establish the concept of quantum memory capacity to evaluate the processing ability in temporal quantum tasks. This study opens opportunities for novel applications with a potential future direction in developing the theoretical magnitude on the quantum time-series processing of quantum devices [39].

In experimental realizations, the measurement protocol on the reservoir for each incident state needs to be repeated many times. This may lead to the effect of back-action, which is the problem of changes in quantum states due to measurement. Each physical implementation can have measures that may successfully work around the problem [40, 41]. For example, one promising solution is considering multiple copies of the same systems, such as a huge ensemble of identical molecules in the nuclear magnetic resonance (NMR) quantum computer [20, 21, 40]. This implementation can provide observable averages for many identical molecules in a solid. Therefore, back-action effects can be neglected because weak measurements are made on the physical substrate. Alternately,

implementations built on a single system without using an ensemble need to be explored in more fruitful applications. One can surpass this challenge by utilizing the shadow tomography protocol to estimate many observables from few projective measurements [42].

This work is supported by MEXT Quantum Leap Flagship Program (MEXT Q-LEAP) Grant Nos. JP-MXS0118067394 and JPMXS0120319794.

* tran_qh@ai.u-tokyo.ac.jp

† k_nakajima@mech.t.u-tokyo.ac.jp

- [1] M. A. Nielsen and I. L. Chuang, *Quantum Computation and Quantum Information: 10th Anniversary Edition*, 10th ed. (Cambridge University Press, USA, 2011).
- [2] M. Mohseni, A. T. Rezakhani, and D. A. Lidar, Quantum-process tomography: Resource analysis of different strategies, *Phys. Rev. A* **77**, 032322 (2008).
- [3] J. L. O’Brien, G. J. Pryde, A. Gilchrist, D. F. V. James, N. K. Langford, T. C. Ralph, and A. G. White, Quantum process tomography of a controlled-not gate, *Phys. Rev. Lett.* **93**, 080502 (2004).
- [4] M. Riebe, K. Kim, P. Schindler, T. Monz, P. O. Schmidt, T. K. Körber, W. Hänsel, H. Häffner, C. F. Roos, and R. Blatt, Process tomography of ion trap quantum gates, *Phys. Rev. Lett.* **97**, 220407 (2006).
- [5] R. C. Bialczak, M. Ansmann, M. Hofheinz, E. Lucero, M. Neeley, A. D. O’Connell, D. Sank, H. Wang, J. Wenner, M. Steffen, A. N. Cleland, and J. M. Martinis, Quantum process tomography of a universal entangling gate implemented with Josephson phase qubits, *Nat. Phys.* **6**, 409 (2010).
- [6] A. Shabani, R. L. Kosut, M. Mohseni, H. Rabitz, M. A. Broome, M. P. Almeida, A. Fedrizzi, and A. G. White, Efficient measurement of quantum dynamics via compressive sensing, *Phys. Rev. Lett.* **106**, 100401 (2011).
- [7] L. C. G. Govia, G. J. Ribeill, D. Ristè, M. Ware, and H. Krovi, Bootstrapping quantum process tomography via a perturbative ansatz, *Nat. Commun.* **11**, 1084 (2020).
- [8] E. Gehrig and O. G. Hess, Spatio-temporal dynamics and fluctuations in quantum dot lasers: mesoscopic theory and modeling, in *Quantum Dot Devices and Computing*, Vol. 4656, edited by J. A. Lott, N. N. Ledentsov, K. J. Malloy, B. E. Kane, and T. W. Sigmon, International Society for Optics and Photonics (SPIE, 2002) pp. 69–78.
- [9] J. E. Martinez, P. Fuentes, P. Crespo, and J. Garcia-Frias, Time-varying quantum channel models for superconducting qubits, *npj Quantum Inf.* **7**, 115 (2021).
- [10] B. Brecht, D. V. Reddy, C. Silberhorn, and M. G. Raymer, Photon temporal modes: A complete framework for quantum information science, *Phys. Rev. X* **5**, 041017 (2015).
- [11] M. G. Raymer and I. A. Walmsley, Temporal modes in quantum optics: then and now, *Physica Scripta* **95**, 064002 (2020).
- [12] H. J. Kimble, The quantum internet, *Nature* **453**, 1023 (2008).
- [13] C. Simon, Towards a global quantum network, *Nat. Photonics* **11**, 678 (2017), 1710.11585.
- [14] S. Wehner, D. Elkouss, and R. Hanson, Quantum internet: A vision for the road ahead, *Science* **362**, eaam9288 (2018).
- [15] See Supplemental Materials for detailed explanations of the reservoir computing, the quantum reservoir computing, the standard quantum process tomography, the temporal tomography, the convergence and metastability analysis of the quantum reservoir, the quantum memory capacity, and other results on the temporal tomography tasks, which include Refs. [43–58].
- [16] H. Jaeger, The “echo state” approach to analysing and training recurrent neural networks-with an erratum note, Bonn, Germany: German National Research Center for Information Technology GMD Technical Report **148**, 13 (2001).
- [17] W. Maass, T. Natschläger, and H. Markram, Real-time computing without stable states: A new framework for neural computation based on perturbations, *Neural Computation* **14**, 2531 (2002).
- [18] M. Lukoševičius and H. Jaeger, Reservoir computing approaches to recurrent neural network training, *Comput. Sci. Rev.* **3**, 127 (2009).
- [19] K. Nakajima and I. Fischer, eds., *Reservoir Computing: Theory, Physical Implementations, and Applications* (Springer Singapore, Singapore, 2021).
- [20] K. Fujii and K. Nakajima, Harnessing disordered-ensemble quantum dynamics for machine learning, *Phys. Rev. Applied* **8**, 024030 (2017).
- [21] K. Nakajima, K. Fujii, M. Negoro, K. Mitarai, and M. Kitagawa, Boosting computational power through spatial multiplexing in quantum reservoir computing, *Phys. Rev. Applied* **11**, 034021 (2019).
- [22] K. Fujii and K. Nakajima, Quantum reservoir computing: A reservoir approach toward quantum machine learning on near-term quantum devices, in *Reservoir Computing: Theory, Physical Implementations, and Applications*, edited by K. Nakajima and I. Fischer (Springer Singapore, Singapore, 2021) pp. 423–450.
- [23] S. Ghosh, A. Opala, M. Matuszewski, T. Paterek, and T. C. Liew, Quantum reservoir processing, *npj Quantum Inf.* **5**, 1 (2019).
- [24] S. Ghosh, A. Opala, M. Matuszewski, T. Paterek, and T. C. H. Liew, Reconstructing quantum states with quantum reservoir networks, *IEEE Trans. Neural Netw. Learn. Syst.* **32**, 3148 (2020).
- [25] S. Ghosh, K. Nakajima, T. Krisnanda, K. Fujii, and T. C. H. Liew, Quantum Neuromorphic Computing with Reservoir Computing Networks, *Adv. Quantum Technol.*, 2100053 (2021).
- [26] For sufficient training samples, our framework can reconstruct the density matrices, which are positive semidefinite. However, due to statistical fluctuations, there are some cases in which the reconstructed matrix A is not positive semidefinite. We project A onto the spectrahedron to obtain a positive semidefinite matrix \hat{A} such that the trace of \hat{A} is equal to 1 and the Frobenius norm between A and \hat{A} is minimized [59].
- [27] J. Chen and H. I. Nurdin, Learning nonlinear input-output maps with dissipative quantum systems, *Quantum Inf. Process.* **18**, 198 (2019).
- [28] Q. H. Tran and K. Nakajima, Higher-order quantum reservoir computing, *Preprint at arXiv:2006.08999* (2020).

- [29] S. Boyd and L. Chua, Fading memory and the problem of approximating nonlinear operators with volterra series, *IEEE Trans. Circuits Syst.* **32**, 1150 (1985).
- [30] D. Porras and J. I. Cirac, Effective quantum spin systems with trapped ions, *Phys. Rev. Lett.* **92**, 207901 (2004).
- [31] K. Kim, M.-S. Chang, R. Islam, S. Korenblit, L.-M. Duan, and C. Monroe, Entanglement and tunable spin-spin couplings between trapped ions using multiple transverse modes, *Phys. Rev. Lett.* **103**, 120502 (2009).
- [32] P. Jurcevic, B. P. Lanyon, P. Hauke, C. Hempel, P. Zoller, R. Blatt, and C. F. Roos, Quasiparticle engineering and entanglement propagation in a quantum many-body system, *Nature* **511**, 202 (2014).
- [33] The channels Ω_n can be considered quantum noises applying to the input states where there is a temporal correlation in these noises. The sequence $\{p_n\}$ resembles the NARMA benchmark [60], which is commonly used for evaluating the computational capability of temporal processing with long time dependence. The sequence $\{u_n\}$ is randomly generated with the same random seed used for generating the input sequence $\{\beta_n\}$; therefore, $\{p_n\}$ depends on $\{\beta_n\}$.
- [34] In the classical baseline method, we assume that we can obtain full tomography of input states, which is not required in our method. Instead of using the measurement results in the quantum reservoir, reservoir state \mathbf{x}_n is constructed directly from the vector form of β_n by stacking the real and imaginary parts in the corresponding density matrix. The readout map and training process are the same as our method.
- [35] H. Jaeger, Short term memory in echo state networks (GMD-Forschungszentrum Informationstechnik, 2001) p. 60.
- [36] G. J. Székely, M. L. Rizzo, and N. K. Bakirov, Measuring and testing dependence by correlation of distances, *Ann. Stat.* **35**, 2769 (2007).
- [37] R. Martínez-Peña, G. L. Giorgi, J. Nokkala, M. C. Soriano, and R. Zambrini, Dynamical phase transitions in quantum reservoir computing, *Preprint at arXiv:2103.05348* (2021).
- [38] Our theoretical investigation is not limited to quantum spin networks, but is more generally associated with the spectrum analysis of reduced dynamics maps. Furthermore, the intriguing results in QMC under varying model parameters remind us of the well-known phenomenon in classical RC called the edge of chaos, where in some situations, a memory capacity achieves the maximum values at the edge of stability between different dynamics regimes [61–63].
- [39] P. Mujal, R. Martínez-Peña, J. Nokkala, J. García-Beni, G. L. Giorgi, M. C. Soriano, and R. Zambrini, Opportunities in quantum reservoir computing and extreme learning machines, *Adv. Quantum Technol.*, 2100027 (2021).
- [40] M. Negoro, K. Mitarai, K. Nakajima, and K. Fujii, Toward NMR quantum reservoir computing, in *Reservoir Computing: Theory, Physical Implementations, and Applications*, edited by K. Nakajima and I. Fischer (Springer Singapore, Singapore, 2021) pp. 451–458.
- [41] J. Chen, H. I. Nurdin, and N. Yamamoto, Temporal information processing on noisy quantum computers, *Phys. Rev. Applied* **14**, 024065 (2020).
- [42] H.-Y. Huang, R. Kueng, and J. Preskill, Predicting many properties of a quantum system from very few measurements, *Nat. Phys.* **16**, 1050 (2020), 2002.08953.
- [43] J. Nokkala, R. Martínez-Peña, G. L. Giorgi, V. Parigi, M. C. Soriano, and R. Zambrini, Gaussian states of continuous-variable quantum systems provide universal and versatile reservoir computing, *Commun. Phys.* **4**, 53 (2021).
- [44] L. C. G. Govia, G. J. Ribeill, G. E. Rowlands, H. K. Krovi, and T. A. Ohki, Quantum reservoir computing with a single nonlinear oscillator, *Preprint at arXiv:2004.14965* (2020).
- [45] S. Dasgupta, K. E. Hamilton, and A. Banerjee, Designing a NISQ reservoir with maximal memory capacity for volatility forecasting, *Preprint at arXiv:2004.08240* (2020).
- [46] D. S. Abrams and S. Lloyd, Quantum algorithm providing exponential speed increase for finding eigenvalues and eigenvectors, *Phys. Rev. Lett.* **83**, 5162 (1999).
- [47] B. I. Bantysh, A. Y. Chernyavskiy, and Y. I. Bogdanov, Quantum tomography benchmarking, *Preprint at arXiv:2012.15656* (2020).
- [48] Y. Quek, S. Fort, and H. K. Ng, Adaptive quantum state tomography with neural networks, *npj Quantum Inf.* **7**, 105 (2021).
- [49] L. Bruneau, A. Joye, and M. Merkli, Infinite products of random matrices and repeated interaction dynamics, *Ann. Inst. H. Poincaré Probab. Statist.* **46**, 442 (2010).
- [50] I. Nechita and C. Pellegrini, Random repeated quantum interactions and random invariant states, *Probab. Theory Relat. Fields* **152**, 299 (2010).
- [51] R. Movassagh and J. Schenker, An ergodic theorem for homogeneously distributed quantum channels with applications to matrix product states, *Preprint at arXiv:1909.11769* (2019).
- [52] R. Movassagh and J. Schenker, Theory of ergodic quantum processes, *Preprint at arXiv:2004.14397* (2020).
- [53] J. M. Steele, Kingman’s subadditive ergodic theorem, *Ann. Inst. H. Poincaré Probab. Statist.* **25**, 93 (1989).
- [54] H. Hennion, Limit theorems for products of positive random matrices, *Ann. Probab.* **25**, 1545 (1997).
- [55] K. Macieszczak, M. Guță, I. Lesanovsky, and J. P. Garrahan, Towards a theory of metastability in open quantum dynamics, *Phys. Rev. Lett.* **116**, 240404 (2016).
- [56] J. B. Lasserre, A trace inequality for matrix product, *IEEE Trans. Autom. Control.* **40**, 1500 (1995).
- [57] J. Dambre, D. Verstraeten, B. Schrauwen, and S. Massar, Information processing capacity of dynamical systems, *Sci. Rep.* **2**, 514 (2012).
- [58] B. Misra and E. C. G. Sudarshan, The Zeno’s paradox in quantum theory, *J. Math. Phys.* **18**, 756 (1977).
- [59] Y. Chen and X. Ye, Projection onto a simplex, *Preprint at arXiv:1101.6081* (2011).
- [60] A. Atiya and A. Parlos, New results on recurrent network training: unifying the algorithms and accelerating convergence, *IEEE Trans. Neural Netw. Learn. Syst.* **11**, 697 (2000).
- [61] N. Bertschinger and T. Natschläger, Real-time computation at the edge of chaos in recurrent neural networks, *Neural Computation* **16**, 1413 (2004).
- [62] T. Toyozumi and L. F. Abbott, Beyond the edge of chaos: Amplification and temporal integration by recurrent networks in the chaotic regime, *Phys. Rev. E* **84**, 051908 (2011).
- [63] T. Haruna and K. Nakajima, Optimal short-term memory before the edge of chaos in driven random recurrent networks, *Phys. Rev. E* **100**, 062312 (2019).

Supplementary Material for “Learning Temporal Quantum Tomography”

Quoc Hoan Tran^{1,*} and Kohei Nakajima^{1,2,†}

¹*Graduate School of Information Science and Technology,
The University of Tokyo, Tokyo 113-8656, Japan*

²*Next Generation Artificial Intelligence Research Center,
The University of Tokyo, Tokyo 113-8656, Japan*

(Dated: December 24, 2024)

This supplementary material describes in detail the calculations, the experiments introduced in the main text, and the additional figures. The equation, figure, and table numbers in this section are prefixed with S (e.g., Eq. (S1) or Fig. S1, Table S1), while numbers without the prefix (e.g., Eq. (1) or Fig. 1, Table 1) refer to items in the main text.

CONTENTS

| | |
|---|----|
| I. Learning the Temporal Tomography | 2 |
| A. Reservoir Computing | 2 |
| B. Quantum Reservoir Computing | 3 |
| C. Standard Quantum Process Tomography | 3 |
| D. Learning the Temporal Tomography | 5 |
| II. Convergence analysis | 5 |
| III. Metastability analysis | 8 |
| IV. Quantum memory capacity | 12 |
| V. Results on the temporal tomography tasks | 15 |
| References | 19 |

arXiv:2103.13973v3 [quant-ph] 6 Sep 2021

* tran.qh@ai.u-tokyo.ac.jp

† k_nakajima@mech.t.u-tokyo.ac.jp

I. LEARNING THE TEMPORAL TOMOGRAPHY

The proposed framework for learning the temporal tomography is a quantum extension of the classical reservoir computing (RC) to deal with quantum tasks. In this section, we first explain the principle of RC and then introduce some quantum extensions of RC in a scheme called quantum reservoir computing (QRC).

A. Reservoir Computing

Within machine learning (ML), the reservoir computing (RC) paradigm is a particular form of classical recurrent neural networks with random connectivity that can generate high-dimensional trajectories [1–3]. The crucial principle of RC is based on the modeling for the representation of the input sequence by feeding the input into a dynamical system called *the reservoir* to encode all relevant nonlinear dynamics. The reservoir is connected to the output by the *readout* part; only connections in this part are trained without affecting the reservoir dynamics. The RC paradigm is based on the following assumption: no knowledge of the system model, a large collection of measurement of readout, and the possibility to predict the target from the states encoded by the reservoir. Furthermore, the training mechanism is straightforward and computationally efficient, allowing RC to become particularly suitable for hardware implementations in various physical systems [4].

We briefly explain here the standard pipeline of RC. In a general picture, the information processing in RC is described by the input-driven map $G : \mathcal{S} \times \mathcal{X} \rightarrow \mathcal{X} \subset \mathbb{R}^K$, where \mathcal{S} and \mathcal{X} are the input and the reservoir's state space, respectively. If we consider an infinite discrete-time input sequence $\{\dots, \mathbf{s}_{-1}, \mathbf{s}_0, \mathbf{s}_1, \dots\}$ fed into the reservoir, the reservoir state \mathbf{x}_n is represented by the following recurrent relation:

$$\mathbf{x}_n = G(\mathbf{s}_n, \mathbf{x}_{n-1}). \quad (\text{S1})$$

In this way, the sequence $\{\dots, \mathbf{x}_{-1}, \mathbf{x}_0, \mathbf{x}_1, \dots\}$ is the nonlinear transformation of the input sequence via the input-driven map implemented by a dynamical system. Therefore, the training in ML tasks can be separated to the reservoir so that we can reduce the computational cost by selecting a simple training procedure.

The RC paradigm can be used for both temporal and non-temporal supervised learning tasks. In temporal supervised learning tasks, we are given an input sequence $\{\mathbf{s}_1, \dots, \mathbf{s}_L\}$ and the corresponding target sequence $\hat{\mathbf{y}} = \{\hat{\mathbf{y}}_1, \dots, \hat{\mathbf{y}}_L\}$ where $\hat{\mathbf{y}}_k \in \mathbb{R}^d$ with d is the output dimension. An RC system with temporal information processing ability includes a readout map $h : \mathcal{X} \rightarrow \mathbb{R}^d$, where the output signal \mathbf{y}_n is simply obtained from the readout map $\mathbf{y}_n = h(\mathbf{x}_n)$ such that $\mathbf{y}_n \approx \hat{\mathbf{y}}_n$ ($n = 1, \dots, L$). The readout map is simply taken as a linear combination of the reservoir states as $\mathbf{y}_n = h(\mathbf{x}_n) = \mathbf{w}^\top \mathbf{x}_n$, where \mathbf{w} is the parameter and needs to be optimized. The training to adjust \mathbf{w} is performed by minimizing the error such as the mean-square error between \mathbf{y}_n and $\hat{\mathbf{y}}_n$ over $n = 1, \dots, L$:

$$\text{MSE} = \frac{1}{L} \sum_{n=1}^L \|\mathbf{y}_n - \hat{\mathbf{y}}_n\|_2^2, \quad (\text{S2})$$

where $\|\cdot\|_2$ denotes the Euclidean norm between two vectors in \mathbb{R}^d . For optimal training, a constant bias term $x_{n,K+1} = 1$ is added to the reservoir state \mathbf{x}_n . A conventional approach is to optimize \mathbf{w} via the linear regression $\hat{\mathbf{Y}} = \mathbf{X}\mathbf{w}$, where $\hat{\mathbf{Y}} = [\hat{\mathbf{y}}_1 \dots \hat{\mathbf{y}}_L]^\top$ is the $L \times d$ target matrix and \mathbf{X} is the $L \times (K+1)$ matrix that combines reservoir states $\mathbf{x}_1, \mathbf{x}_2, \dots, \mathbf{x}_L$ of training data. The optimal value of \mathbf{w} is obtained via the Ridge regression in the matrix form $\hat{\mathbf{w}}^\top = (\mathbf{X}^\top \mathbf{X} + \eta \mathbf{I})^{-1} \mathbf{X}^\top \hat{\mathbf{Y}}$. Here, η is a positive constant shifting the diagonals introduced to avoid the problem of the near-singular moment matrix. The trained parameter $\hat{\mathbf{w}}$ is used to generate outputs in the situation where we do not know about the target sequence and can only access the input sequence.

The information processing via the input-driven map is similar in non-temporal learning tasks, but the target in non-temporal ones is not the sequence but a specific value such as a label or an output vector corresponding with given input data. The input data are firstly converted into a sequence to be fed into the reservoir, then the reservoir states obtained from the reservoir dynamics are considered nonlinear features to learn the mapping to the output. The learning task can be regression or classification with respect to the property of output set as dense or discrete, respectively. In this way, the loss function measuring the prediction error can be designed in a flexible way in which we can apply more complicated training algorithms such as support vector machine or heuristic search methods to nonlinear optimization problems.

B. Quantum Reservoir Computing

Quantum reservoir computing (QRC) is one of proposals to exploit the quantum dynamics as a reservoir. Here, a disordered ensemble quantum dynamics system is used as a computational resource with the possibility of processing with an exponentially large number of degrees of freedom. The crucial idea is using a quantum system for obtaining the input-driven map defined in Eq. (S1). This input-driven map depends on the dynamical evolution of the quantum system and the quantum measurements to extract reservoir states from the system. For example, the reservoir can be implemented by a set of interacting qubits in the NMR system [5, 6], a set of fermions [7–9], a set of interacting quantum harmonic oscillators [10], or even a single nonlinear oscillator driven by a Hamiltonian dynamics [11]. The proof-of-principle experimental demonstrations for QRC are ongoing in the research with promising proposals for the NMR platform [12] and NISQ quantum computers [13, 14].

In our study, we model the QRC approach via the framework of repeated quantum interactions, which can be considered a general approach using the NMR system in Ref. [5]. In the repeated quantum interactions, input sequence is fed via the sequence interactions between reservoir system (called a *reduced quantum reservoir*) \mathcal{S} with a auxiliary system \mathcal{E} . The dynamical evolution is modeled by the following recurrent relation (Eq. 2 in our main text)

$$\rho_n = \mathcal{L}_{\beta_n}(\rho_{n-1}) = \text{Tr}_{\mathcal{E}}[U(\rho_{n-1} \otimes \beta_n)U^\dagger], \quad (\text{S3})$$

where ρ_n, β_n are the states of \mathcal{S} and \mathcal{E} for the n th interaction, respectively. Here, U is an unitary evolution and \mathcal{L}_{β_n} is called the *reduced dynamics map*, which is a completely positive and trace-preserving (CPTP) map acting on the space $\mathcal{M}_{\mathcal{S}}$ of density matrices in \mathcal{S} .

One can ask where the mechanism to obtain the nonlinearity is, since even if the evolution is not unitary we still get linear dynamics. In fact, it has been shown that introducing a coherent nonlinearity to quantum evolution means that we can obtain the ability to solve NP-hard problems [15]. Therefore, a more likely way to introduce nonlinearities is to use projective measurements, which are clearly nonlinear operations using the projectors on the space spanned by the basis of the system used in a measurement. In this way, if a local observable O is described by a collection of projectors $\{P_j\}$ as $O = \sum_j a_j P_j$, where a_j are the values of a physical quantity of a measurement associated with P_j , the probability to obtain the measurement result a_j is given by $p(a_j) = \text{Tr}[P_j \rho]$. Then, the expectation value of the physical quantity is given by

$$\sum_j a_j p(a_j) = \sum_j a_j \text{Tr}[P_j \rho] = \text{Tr}[O \rho] = \langle O \rangle_{\rho}. \quad (\text{S4})$$

We obtain partial information regarding the state ρ_n of the quantum system \mathcal{S} after the n th interaction with the environment by measuring local observables O_1, O_2, \dots, O_K on the state of \mathcal{S} . Then, the k th element x_{nk} of the reservoir states \mathbf{x}_n can be calculated as the expectation of the measurement results via O_k on ρ_n :

$$x_{nk} = \text{Tr}[O_k \rho_n] = \langle O_k \rangle_{\rho_n}. \quad (\text{S5})$$

One can increase the dimension of \mathbf{x}_n by performing measurements at multiple times. Between two inputs, M cycles of the unitary evolution are processed and each of them is followed by a measurement. M is called the measurement multiplexity. Thus we obtain MK elements in each reservoir state. After obtaining the reservoir states, the training procedure in QRC is similar to the classical RC.

We note that we can also construct a universal quantum reservoir consisting of multiple and non-interacting quantum reservoirs \mathcal{S} . For example, let us consider a quantum system \mathcal{S} consisting of two non-interacting reduced quantum reservoirs \mathcal{S}_a and \mathcal{S}_b with the corresponding reduced dynamics maps \mathcal{L}_a and \mathcal{L}_b , respectively. Since \mathcal{S}_a and \mathcal{S}_b are not interacting, a quantum state ρ in \mathcal{S} can be displayed as a tensor product

$$\rho = \rho_a \otimes \rho_b, \quad (\text{S6})$$

where ρ_a and ρ_b are two quantum states in \mathcal{S}_a and \mathcal{S}_b , respectively. Then, the reduced dynamics map \mathcal{L} acting on the space $\mathcal{M}_{\mathcal{S}}$ can be defined as

$$\rho = \rho_a \otimes \rho_b \rightarrow \mathcal{L}(\rho) = \mathcal{L}_a(\rho_a) \otimes \mathcal{L}_b(\rho_b). \quad (\text{S7})$$

C. Standard Quantum Process Tomography

Before going into the details of learning the temporal tomography, we explain standard quantum process tomography (standard QPT). The following explanation is referenced from Refs. [16, 17].

Suppose $\Omega(\cdot)$ is a time-independent quantum channel, which is a completely-positive linear and trace-preserving map from a D_A -dimensional Hilbert space \mathcal{H}_A to a D_B -dimensional Hilbert space \mathcal{H}_B (for notational simplicity, we take $\mathcal{H}_A \equiv \mathcal{H}_B \equiv \mathcal{H}$ and $D_A = D_B = D$). In principle, $\Omega(\cdot)$ can be reconstructed from the measurement data using a proper inversion, since $\Omega(\cdot)$ is a linear map. A time-independent $\Omega(\cdot)$ can be described using a set of D^2 time-independent operators $\{E_k\}_{k=1}^{D^2}$ such that $\sum_{k=1}^{D^2} E_k^\dagger E_k = I$ and

$$\Omega(\rho) = \sum_{k=1}^{D^2} E_k \rho E_k^\dagger \quad (\text{S8})$$

for an arbitrary $D \times D$ -dimensional density matrix ρ . To determine E_k from measurement data, it is convenient to choose a description using a basis set of operators $\{\tilde{E}_k\}_{k=1}^{D^2}$ for the space of $D \times D$ -dimensional linear operators. In this case, $E_k = \sum_{m=1}^{D^2} e_{km} \tilde{E}_k$ for D^2 complex numbers e_{km} . Then, Eq. (S8) becomes

$$\Omega(\rho) = \sum_{mn} \tilde{E}_m \rho \tilde{E}_m^\dagger \chi_{mn}, \quad (\text{S9})$$

where $\chi_{mn} = \sum_k e_{km} e_{kn}^*$.

If the basis set of operators $\{\tilde{E}_k\}$ is fixed, then the quantum channel Ω can be described by a D^4 -dimensional complex number vector $\chi = (\chi_{mn})$ (called the superoperator). However, due to the completeness relation $\sum_{k=1}^{D^2} E_k^\dagger E_k = I$, we only need $D^4 - D^2$ independent parameters to describe χ . The idea determining χ is to prepare D^2 linearly independent inputs (as the basis set of operators for the space of $D \times D$ operators) $\{\rho_k\}_{k=1}^{D^2}$ and perform state tomography for the outputs states $\Omega(\rho_k)$. In this case, we often choose $\tilde{E}_k = \rho_k$ since ρ_k are Hermitian operators and valid observables.

Considering an orthonormal basis $\{|m\rangle\}_{m=0}^{D-1}$ of \mathcal{H} , a convenience choice for input states is $\rho_k = |m\rangle\langle n|$. Given $|+\rangle = \frac{|m\rangle+|n\rangle}{\sqrt{2}}$ and $|-\rangle = \frac{|m\rangle+i|n\rangle}{\sqrt{2}}$, we can express the coherence $|m\rangle\langle n|$ as

$$|m\rangle\langle n| = |+\rangle\langle +| + |-\rangle\langle -| - \frac{(1+i)}{2} (|m\rangle\langle m| + |n\rangle\langle n|). \quad (\text{S10})$$

Therefore, from the experimental measurements of $\Omega(|m\rangle\langle m|)$, $\Omega(|n\rangle\langle n|)$, and $\Omega(|+\rangle\langle +|)$ and $\Omega(|-\rangle\langle -|)$, we can determine $\Omega(|m\rangle\langle n|)$ due to the linearity of Ω .

We note that every $\Omega(\rho_k)$ can be expressed as a linear combination of the basis states, as

$$\Omega(\rho_k) = \sum_l \lambda_{kl} \rho_l. \quad (\text{S11})$$

Here, parameters λ_{kl} contain the measurement results and can be calculated from state tomography experiments as $\lambda_{kl} = \text{Tr}[\tilde{E}_k \Omega(\rho_l)]$ (since we choose $\tilde{E}_k = \rho_k$). Generally, we can write

$$\tilde{E}_m \rho_k \tilde{E}_n^\dagger = \sum_l B_{mn, lk} \rho_l, \quad (\text{S12})$$

where the $D^4 \times D^4$ -dimensional matrix $\mathbf{B} = (B_{mn, lk})$ is determined by the fixed choice of bases $\{\rho_k\}$ and $\{\tilde{E}_k\}$. Combining Eq. (S9), Eq. (S11), and Eq. (S12), we have

$$\sum_l \sum_{mn} \chi_{mn} B_{mn, lk} \rho_l = \sum_l \lambda_{kl} \rho_l. \quad (\text{S13})$$

From the linear independence of the ρ_l , it follows that, for each k , we have $\sum_{mn} B_{mn, lk} \chi_{mn} = \lambda_{kl}$, or in the matrix form $\mathbf{B}\chi = \boldsymbol{\lambda}$, where $\boldsymbol{\lambda}$ is the D^4 -dimensional vector created from $\{\lambda_{kl}\}$. Therefore, the superoperator χ can be described by a proper linear conversion (since we know \mathbf{B} and $\boldsymbol{\lambda}$).

In the standard QPT explained above, we must prepare D^2 independent inputs $\{\rho_k\}$ and perform quantum-state tomography for the corresponding outputs $\{\Omega(\rho_k)\}$. For each ρ_k , we must measure the expectation value of the D^2 fixed-basis operators $\{\tilde{E}_k\}$ in the state $\Omega(\rho_k)$ that requires a number copies of $\Omega(\rho_k)$ to obtain a fixed precision for χ . Therefore, the total number of required measurements for standard QPT is $O(D^4)$. Here, we use the term measurement with the implicit meaning of the measurement on an ensemble of identically prepared quantum systems corresponding to a given experimental setting. Furthermore, to solve the linear system $\mathbf{B}\chi = \boldsymbol{\lambda}$, we need a huge classical resource to do the inversion of the $D^4 \times D^4$ -dimensional matrix \mathbf{B} .

D. Learning the Temporal Tomography

A significant difference in the applications of QRC approaches compared with the conventional RC is the ability to deal with quantum tasks such as the classification of quantum states as entangled or separable [7], the quantum tomography [8], and the quantum state preparation [9]. While some of the QRC approaches are not proposed for quantum tasks [5, 10, 11], the current proposals of QRC for quantum tasks focused on a static quantum state, which is coupled to the reservoir [7, 8]. Here, our approach based on repeated quantum interactions provides the ability to perform quantum tasks for a sequence of input quantum states where the outputs of these tasks depend on the past input states.

We explain the setting for the temporal quantum map \mathcal{F} to see the basic difference with the standard QPT. Given a sequence of input quantum states β_1, β_2, \dots , a quantum device processes this input sequence via a temporal map \mathcal{F} , where the corresponding output states are $\mathcal{F}(\beta_1), \mathcal{F}(\beta_2), \dots$. We assume that the output $\mathcal{F}(\beta_n)$ may depend on $\mathcal{F}(\beta_{n-1})$ and a finite number of past inputs. We can think that the action of \mathcal{F} to the input sequence is equivalent to a function of current and past inputs, which is often seen in classical time-series processing. The density matrix of $\mathcal{F}(\beta_n)$ can be reconstructed if we can model this action to an accessible input sequence, that is to model the dependency of the current output to the current and past inputs. This is different with the standard QPT, which requires an accessible resource with D^2 independent input states and the corresponding D^2 output states to find the general form of the linear map.

In addition, Fig. 1(a) in our main text helps the readers capture the visual concept of the quantum map \mathcal{F} . Here, we consider a stream of unknown quantum channels $\{\Omega_n\}$ applied to the input stream where there is a dependency between these channels. We note that \mathcal{F} is generally not a standard quantum channel, but the output of \mathcal{F} at each time in the output stream is considered as a mixed state of a finite number of current and past channel's outputs as (Eq. (1) in the main text)

$$\mathcal{F}(\beta_n) = \frac{1}{Z} \sum_{i=0}^d \eta_i \Omega_{n-i}(\beta_{n-i}). \quad (\text{S14})$$

Here, η_i are unknown non-negative real numbers with $Z = \sum_{i=0}^d \eta_i$ to preserve the trace. This concept of \mathcal{F} envisions a typical case in the future realization of quantum communication and quantum internet where quantum data can be transmitted via time-dependent quantum channels under a time-delayed effect. The density matrix of $\mathcal{F}(\beta_n)$ can only be reconstructed if we can model the action of \mathcal{F} to the input sequence.

In learning the tomography of the temporal quantum map \mathcal{F} , we are given an input sequence of states $\{\beta_1, \dots, \beta_L\}$ and the corresponding target sequence $\hat{\mathbf{y}} = \{\hat{\mathbf{y}}_1, \dots, \hat{\mathbf{y}}_L\}$, where $\hat{\mathbf{y}}_k$ is the real vector form to stack the real and imaginary elements of $\mathcal{F}(\beta_k)$. In the evaluation stage, we are given an input sequence $\{\beta_{L+1}, \dots, \beta_{L+T}\}$ with the corresponding target $\{\hat{\sigma}_{L+1}, \dots, \hat{\sigma}_{L+T}\}$, where $\hat{\sigma}_i = \mathcal{F}(\beta_i)$. The reconstructed output sequence is $\{\mathbf{y}_{L+1}, \dots, \mathbf{y}_{L+T}\}$, which is rearranged in the matrix form $\{\sigma_{L+1}, \dots, \sigma_{L+T}\}$. Due to statistical fluctuations, there are some cases in which the reconstructed matrix σ_i is not positive semidefinite. We project σ_i onto the spectrahedron to obtain a positive semidefinite matrix σ'_i such that the trace of σ'_i is equal to 1 and the Frobenius norm between σ_i and σ'_i is minimized [18]. This technique is considered as *projected pseudo-inversion estimator*. Other proposals for a density matrix estimator can be found in a survey in Ref. [19].

Regarding the learning mechanism, we assume that we have full tomography for the corresponding output states of \mathcal{F} in the learning and evaluation phase. Note that the evaluation phase is performed for evaluating the appropriate values of model parameters but is not needed after the model parameters are fixed. The condition for accessible full tomography in the training phase is common and unavoidable in implementing supervised learning methods in quantum tomography, for example, in Refs. [8, 20]. However, this does not defeat the potential advantage of our proposal. After the training procedure, we are able to reconstruct the output $\mathcal{F}(\beta_n)$ in the sequence by only using a single process of measurements in the reservoir. This is performed without reconfiguring the experimental setup or doing full tomography with a number of identical copies of $\mathcal{F}(\beta_n)$ for every n . Our framework is general and can be applied for different types of the temporal quantum map \mathcal{F} without reconfiguring the measurement bases. Those points are significant contributions of our proposal.

II. CONVERGENCE ANALYSIS

Since \mathcal{F} can be considered as a function of past sequences of input quantum states, the framework to learn \mathcal{F} should have the ability to retain information about recent inputs in their activity. This property in the classical context is known as the fading memory property, mentioned by S. Boyd and L. Chua [21]. The reservoir needs to

forget its initial state to ensure the fading memory property. If the effect of the initial state in the reservoir is strong, the response of the reservoir to the same input sequence may be different if the reservoir starts from two different initial states. This effect may result in the loss of reproducibility in temporal processing tasks. Therefore, a quantum system with a reproducible temporal information processing ability must produce the trajectories that are robust to small perturbations to the system, i.e., the computations for the same input sequence are independent of its initial state. We refer to this as quantum echo state property (QESP), which is defined in Ref. [22] and mentioned in the convergence property of dissipative quantum systems in Ref. [23].

Definition S1. *A quantum system used in temporal information processing tasks is said to satisfy the quantum echo state property (QESP) with respect to the distance \mathcal{D} between quantum states if for any input sequence of length L , it holds that $\mathcal{D}(\rho_L^{(1)}, \rho_L^{(2)}) \rightarrow 0$ as $L \rightarrow \infty$, where $\rho_L^{(1)}, \rho_L^{(2)}$ are the states after L steps corresponding with different initial states $\rho_0^{(1)}, \rho_0^{(2)}$.*

In the following parts, we consider \mathcal{D} as the trace distance, or the Schatten 1-norm, defined by $\mathcal{D}(\rho, \rho') = \|\rho - \rho'\| = \text{Tr}[\|\rho - \rho'\|]$ between quantum states ρ and ρ' , where we define $|A| = \sqrt{A^\dagger A}$ to be the positive square root of $A^\dagger A$ for any matrix A . Since a CPTP map is a contracting map w.r.t. the trace distance, the density matrices in quantum repeated interactions satisfy decreasing system distinguishability [16] as

$$\|\rho_n^{(1)}, \rho_n^{(2)}\| \leq \|\rho_{n-1}^{(1)}, \rho_{n-1}^{(2)}\|, \quad (\text{S15})$$

where $\rho_n^{(1)}, \rho_n^{(2)}$ are the states after n interactions corresponding with different initial states $\rho_0^{(1)}, \rho_0^{(2)}$. We denote $\Phi_n = \mathcal{L}_{\beta_n} \mathcal{L}_{\beta_{n-1}} \dots \mathcal{L}_1$, then Φ_n is a CPTP map and $\rho_n = \Phi_n(\rho_0)$. We are interested in the action of Φ_n to study the dynamics of \mathcal{S} , particularly in asymptotic behavior in the limit $n \rightarrow \infty$.

Since the reduced dynamics maps \mathcal{L}_{β_n} do not have in general a common invariant state, we firstly investigate the behavior of the reservoir at ergodic limits. We use here the results developed in Ref. [24] (Theorem 1.3) and Ref. [25] (Theorem 5.2, Proposition 6.3) to get the following result.

Result S1 (Ergodicity of the reduced quantum reservoir). *Let $\{\beta_n\}$ be a sequence of i.i.d. random quantum states under the main hypothesis that the induced CPTP maps \mathcal{L}_{β_n} have a unique invariant state. Then, for all initial states ρ_0 , the reduced quantum reservoir \mathcal{S} satisfies the ergodic limit*

$$\lim_{N \rightarrow \infty} \frac{1}{N} \sum_{n=1}^N \rho_n = \lim_{N \rightarrow \infty} \frac{1}{N} \Phi_n(\rho_0) = \rho_{\text{es}}, \quad (\text{S16})$$

where $\rho_{\text{es}} \in \mathcal{M}_{\mathcal{S}}$ is the unique invariant state of the deterministic map $\mathcal{L}_{\mathbb{E}[\beta]}$.

Next, motivated by the theory of ergodic quantum processes in Refs. [26, 27], we derive the following theorem as a sufficient condition for the QESP of a QR.

Result S2. *The quantum reservoir \mathcal{S} satisfies the quantum echo state property if the input sequence $\{\beta_n\}$ is a random ergodic sequence under the main hypothesis that for some n , Φ_n is a strictly positive CPTP map with a positive probability. Here, a CPTP map $\mathcal{L} : \mathcal{M}_{\mathcal{S}} \rightarrow \mathcal{M}_{\mathcal{S}}$ is called strictly positive if it sends every positive semidefinite matrix in $\mathcal{M}_{\mathcal{S}}$ to a positive definite matrix.*

Proof.— Since $\{\beta_n\}$ is an ergodic sequence the sequence of \mathcal{L}_{β_n} is also ergodic. We drop the notion β for an easy description of the reduced dynamics maps \mathcal{L}_{β_n} as \mathcal{L}_n . We assume that the sequence of \mathcal{L}_n is drawn from an ensemble Ω . Consider the shift map $\mathcal{T} : \Omega \rightarrow \Omega$ such that $\mathcal{T}(\mathcal{L}_1, \mathcal{L}_2, \dots) = (\mathcal{L}_2, \mathcal{L}_3, \dots)$. Due to the ergodic property, \mathcal{T} is ergodic map, that is, the dynamics generated by \mathcal{T} starting from a typical sequence will cover Ω with full measure. We can write the composition form as

$$\mathcal{L}_{m+n} \dots \mathcal{L}_{m+1} = \mathcal{T}^m \circ \Phi_n, \quad (\text{S17})$$

for any $n, m \geq 1$.

For a CPTP map $\mathcal{L} : \mathcal{M}_{\mathcal{S}} \rightarrow \mathcal{M}_{\mathcal{S}}$, let $c(\mathcal{L})$ be the smallest number such that $\|\mathcal{L}(\rho) - \mathcal{L}(\sigma)\| \leq c(\mathcal{L})\|\rho - \sigma\|$ for any $\rho, \sigma \in \mathcal{M}_{\mathcal{S}}$. Because \mathcal{L} is contracting w.r.t. $\|\cdot\|$, such $c(\mathcal{L})$ (called the *contraction coefficient* of \mathcal{L}) always exists and $0 < c(\mathcal{L}) \leq 1$. We denote $c_n = c(\Phi_n)$ and have the following inequalities:

$$c(\Phi_{m+n}) \leq c(\Phi_m) c(\mathcal{L}_{m+n} \dots \mathcal{L}_{m+1}) \quad (\text{S18})$$

$$\ln(c(\Phi_{m+n})) \leq \ln(c(\Phi_m)) + \ln(c(\mathcal{L}_{m+n} \dots \mathcal{L}_{m+1})) \quad (\text{S19})$$

$$\ln(c(\Phi_{m+n})) \leq \ln(c(\Phi_m)) + \ln(c(\mathcal{T}^m \circ \Phi_n)) \quad (\text{S20})$$

As $\ln(c(\Phi_n)) \leq 0$, the subadditive ergodic theorem guarantees [28] that the following limit exists:

$$\lim_{n \rightarrow \infty} \frac{1}{n} \ln(c(\Phi_n)) = \kappa, \quad (\text{S21})$$

where $\kappa \leq 0$ is given by the limit of expectations over Ω (Ref. [29], Lemma 3.2)

$$\kappa = \lim_{n \rightarrow \infty} \frac{1}{n} \mathbb{E}[\ln(c(\Phi_n))] = \inf_n \frac{1}{n} \mathbb{E}[\ln(c(\Phi_n))]. \quad (\text{S22})$$

By the hypothesis of the strictly positive map, for some n we have $c(\Phi_n) < 1$ with a positive probability. Therefore, there exists $n \geq 1$ such that $-\infty \leq \frac{1}{n} \mathbb{E}[\ln(c(\Phi_n))] < 0$, thus $\kappa < 0$. From Eq. (S21), there exists a positive $\mu < 1$, a constant $A > 0$, and $n_0 \geq 1$ such that $c(\Phi_n) \leq A\mu^n$ for all $n \geq n_0$. Then,

$$\|\rho_n^{(1)} - \rho_n^{(2)}\| = \|\Phi_n(\rho_0^{(1)}) - \Phi_n(\rho_0^{(2)})\| \leq c(\Phi_n) \|\rho_0^{(1)} - \rho_0^{(2)}\| \leq A\mu^n \|\rho_0^{(1)} - \rho_0^{(2)}\| \quad (\text{S23})$$

for all $n \geq n_0$, thus $\|\rho_n^{(1)} - \rho_n^{(2)}\| \rightarrow 0$ as $n \rightarrow \infty$. Therefore, we obtain the QESP. Furthermore, if the system starts from two different states, then the trace distance between the states will decay exponentially to zero.

In some practical situations, result S2 may be too restrictive to be used. We can relax the definition S1 as the following definition.

Definition S2. Given a positive ε , a quantum reservoir is said to satisfy the ε -QESP if for any input sequence there exists a smallest number $T(\varepsilon)$ such that $\|\Phi_n(\rho_0^{(1)}) - \Phi_n(\rho_0^{(2)})\| < \varepsilon$ for all $n \geq T(\varepsilon)$ and all different initial states $\rho_0^{(1)}$, $\rho_0^{(2)}$. The maximum $T(\varepsilon)$ for all input sequences is defined as the ε -QESP time scale of the quantum reservoir.

The ε -QESP time scale indicates the number of time steps that the quantum reservoir must wait to forget its initial state. If we can evaluate this quantity, we can know when to start the learning process after a number of transient time steps. We demonstrate that the ε -QESP and the corresponding time scale can be evaluated via the spectrum of the reduced dynamics maps \mathcal{L}_n . First, we consider the case of the constant input $\beta_n = \beta$ for all n . We have $\mathcal{L}_n \equiv \mathcal{L}$ for all n and $\rho_n = \mathcal{L}^n(\rho_0)$. Any density matrix can be converted into the vector form, which allows us to define a linear space of matrices (Fock-Liouville space) associated with an inner product. Consider an arbitrary density matrix $\rho = \sum_{i,j} \rho_{i,j} |i\rangle\langle j|$. We can write its vectorized form using the Choi-Jamiolkowski isomorphism as $\text{vec}(\rho) = \sum_{i,j} \rho_{i,j} |j\rangle \otimes |i\rangle$, which is the same as stacking columns of ρ . The reduced dynamics map \mathcal{L} can now be expressed as a matrix $\tilde{\mathcal{L}}$, such that $\text{vec}(\rho_n) = \tilde{\mathcal{L}} \text{vec}(\rho_{n-1})$. The spectrum of \mathcal{L} can be written as $1 = |\lambda_1| \geq |\lambda_2| \geq \dots \geq |\lambda_s|$, where λ_j is the j th eigenvalue of $\tilde{\mathcal{L}}$. Because \mathcal{L} can be a non-Hermitian map, it can have both left and right eigenmatrices. We denote L_j and R_j as the left and right eigenmatrices corresponding to eigenvalue λ_j , respectively. We choose the normalization such that $\text{Tr}(L_k R_l) = \delta_{kl}$ for all $1 \leq k, l \leq s$, and $\text{Tr}[R_1] = 1$ (i.e., L_1 being the identity $L_1 = I$). Since $\text{vec}(\rho_n) = \tilde{\mathcal{L}}^n(\text{vec}(\rho_0))$, we have

$$\text{vec}(\rho_n) = \text{vec}(R_1) + \sum_{j=2}^s b_j \lambda_j^n \text{vec}(R_j), \quad (\text{S24})$$

where $b_j = \text{vec}(L_j)^\dagger \text{vec}(\rho_0) = \text{Tr}[L_j \rho_0]$. Therefore, if $|\lambda_2|^{-1} > 1$, the steady state ρ_{ss} of the system is unique ($\rho_{\text{ss}} = R_1$) with the convergence rate depending on the magnitude of $|\lambda_2|^{-1}$, i.e., $\|\rho_n - \rho_{\text{ss}}\| \sim e^{-n/N}$ with $N \sim \frac{1}{\ln(|\lambda_2|^{-1})}$. The QESP is satisfied that we can evaluate the ε -QESP time scale as $O(\frac{\ln(\varepsilon^{-1})}{\ln(|\lambda_2|^{-1})})$.

Next, we consider the case when the input is a sequence of i.i.d. density matrices. The result S2 provides us the following proposition, which is stated in our main text.

Proposition S1. If there exist n_0 such that $\mu = \max(c_n) < 1$ for all $n \geq n_0$, where $0 < c_n \leq 1$ is the contraction coefficient of \mathcal{L}_{β_n} , then the ε -QESP time scale can be evaluated as $O(\frac{\ln(\varepsilon^{-1})}{\ln(\mu^{-1})})$.

Proof.— In the proof of result S2, for a CPTP map $\mathcal{L} : \mathcal{M}_S \rightarrow \mathcal{M}_S$, the contraction coefficient $c(\mathcal{L})$ denotes the smallest number such that $\|\mathcal{L}(\rho) - \mathcal{L}(\sigma)\| \leq c(\mathcal{L}) \|\rho - \sigma\|$ for any $\rho, \sigma \in \mathcal{M}_S$. Such $c(\mathcal{L})$ always exists and $0 < c(\mathcal{L}) \leq 1$. Since $\mu = \max(c_n) < 1$ for all $n \geq n_0$, we have $c(\Phi_n) \leq A\mu^n < 1$ for some constant A for all $n \geq n_1 \geq n_0$ for some n_1 . Equation (S23) shows us the result in the proposition.

Proposition S1 gives us a consequence that to obtain a sufficient check for the QESP and to know the ε -QESP time scale, we only need to investigate the contracting coefficient via the spectrum of the reduced dynamics map for random inputs.

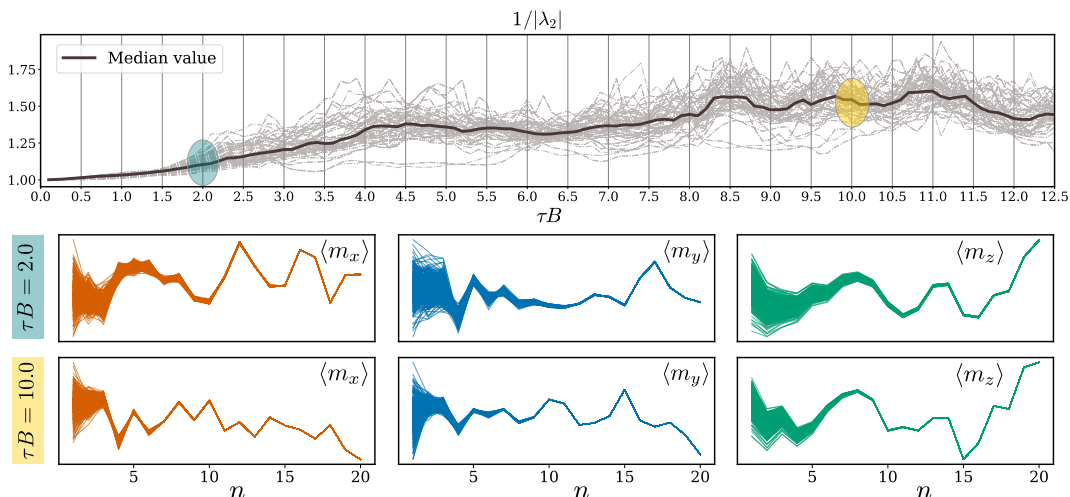


FIG. S1. (Top) The values of $1/|\lambda_2|$ for 100 random reduced dynamics maps \mathcal{L}_β with $N_m = 4, N_e = 2, \alpha = 1, J = 1$, and $J/B = 1$. The solid line depicts the median value of the ensemble of dynamics maps. (Middle and bottom) The trajectories of the average magnetization generated with 500 random initial states of \mathcal{S} at $\tau B = 2.0$ and $\tau B = 10.0$.

To numerically investigate the transient dynamics, we consider a specific system modeled by the transverse field Ising model, where the Hamiltonian is given by

$$H = - \sum_{i>j=1}^N J_{i,j} \hat{s}_i^x \hat{s}_j^x - B \sum_j^N \hat{s}_j^z. \quad (\text{S25})$$

Here, B is the natural frequency of $1/2$ -spins represented for qubits. \hat{s}_j^γ ($\gamma \in \{x, y, z\}$) are the Pauli operators measuring the qubit j along the γ direction, which can be described as an N -tensor product of 2×2 -matrices as

$$\hat{s}_j^\gamma = \mathbf{I} \otimes \dots \otimes \underbrace{\hat{s}_j^\gamma}_{j\text{-index}} \otimes \dots \otimes \mathbf{I}, \quad (\text{S26})$$

where $\mathbf{I} = \begin{bmatrix} 1 & 0 \\ 0 & 1 \end{bmatrix}$, $\hat{s}^x = \begin{bmatrix} 0 & 1 \\ 1 & 0 \end{bmatrix}$, $\hat{s}^y = \begin{bmatrix} 0 & -i \\ i & 0 \end{bmatrix}$, and $\hat{s}^z = \begin{bmatrix} 1 & 0 \\ 0 & -1 \end{bmatrix}$. The coupling coefficients J_{ij} between spins can be randomly selected or fixed depending on the distance of interaction. To describe our QR, we assume that the auxiliary system \mathcal{E} includes the first N_e spins where the remaining $N_m = N - N_e$ spins form the reservoir \mathcal{S} . We present the setting of *power-law decaying* for J_{ij} and frequency B corresponding with the physical implementation in a trapped-ion quantum simulation [30–32]. Here, $J_{ij} = J|i - j|^{-\alpha}/N(\alpha)$ with an interaction strength J , power coefficient $0 < \alpha < 3$, and normalization constant $N(\alpha) = \frac{1}{N-1} \sum_{i>j} |i - j|^{-\alpha}$. The coupled system $(\mathcal{S}, \mathcal{E})$ is a closed system with the total Hamiltonian H unchanged during each interaction. We consider the model parameters $\alpha = 1.0, J = B = 1.0$, and the unitary $U = \exp(-i\tau H)$, where τ is the interaction time.

The top panel of Fig. S1 shows the values of $1/|\lambda_2|$ according to the normalized interaction time τB for 100 random reduced dynamics maps $\mathcal{L}_\beta(\rho) = \text{Tr}_{\mathcal{E}}[U(\rho \otimes \beta)U^\dagger]$ with $N_m = 4, N_e = 2$. Here, β is drawn from an ensemble of Haar random pure states of dimension 2^{N_e} . The QESP is satisfied in values of τB such as all values of $1/|\lambda_2|$ are higher than 1. Furthermore, the higher $1/|\lambda_2|$ leads to the smaller ε -QESP time scale. We then fix a random input sequence and investigate the trajectories of the average magnetization $\langle m_\gamma \rangle = \text{Tr}[\hat{m}_\gamma \rho_n]$, where $\hat{m}_\gamma = \frac{1}{N_m} \sum_j \hat{s}_j^\gamma$ are the average spin operators at $\gamma \in \{x, y, z\}$ directions in \mathcal{S} . The trajectories begin with 500 random initial states of \mathcal{S} . The fluctuations reduce as the number n of interactions increases. This reduction is faster as the ε -QESP scale is smaller, as illustrated in Fig. S1 with $\tau B = 2.0$ and $\tau B = 10.0$.

III. METASTABILITY ANALYSIS

In this section, we derive the metastability of the reservoir dynamics. Metastability is a characteristic feature of the dynamics of a slow relaxing system with the partial relaxation into long-lived states before eventual decay to the

true stationary state. Metastability appears due to the separation of time scales in the dynamics; therefore, different initial states of the system will relax to different metastable states in the transient dynamics before eventual relaxation to the true stationary state. The metastability in open quantum systems has been studied in Ref. [33]. Here, we formulate the metastability in our quantum reservoir framework.

First, we consider the case of constant input $\beta_n = \beta$ for all n . The reduced dynamics map is represented by a fixed CPTP map \mathcal{L} with the spectrum $1 = |\lambda_1| \geq |\lambda_2| \geq \dots |\lambda_s|$, where λ_j is the j th eigenvalue of \mathcal{L} . We observe that each λ_j such that $|\lambda_j| < 1$ represents a time scale of the system. Let us assume that $|\lambda_2| < 1$ and there is a large separation between $|\lambda_m|$ and $|\lambda_{m+1}|$ in the spectrum of \mathcal{L} as $1 = |\lambda_1| \geq \dots |\lambda_m| \gg |\lambda_{m+1}| \geq \dots |\lambda_s|$. This separation corresponds to two scales defined by $N_1 = \frac{1}{\ln(|\lambda_{m+1}|^{-1})}$ and $N_2 = \frac{1}{\ln(|\lambda_m|^{-1})}$. The range $N_1 \ll n \ll N_2$ defines the range where the metastability occurs and the system relaxes into a state in metastable manifold (MM), which we can consider as an effective dimensional reduction. In the metastable regime, the dynamics will be described via the motion in the MM towards the true stationary state, which is reached at $n \gg N_2$.

The MM is a convex subset of the system states on which the long transient dynamics takes place. From Eq. (S24), the projection \mathcal{P} of ρ_n onto the MM is given by

$$\mathcal{P}\rho_n = \rho_{\text{ss}} + \sum_{j=2}^m \text{Tr}[\rho_n L_j] R_j. \quad (\text{S27})$$

The evolution of dynamics in this MM is described by the effective reduced dynamics map $\mathcal{L}_{\text{eff}} = \mathcal{P}\mathcal{L}\mathcal{P}$, which is the projection of \mathcal{L} on the MM. In this sense, MM can be regarded as being $(m-1)$ dimensional simplex, but each point in this manifold represents a density matrix in $\mathcal{M}_{\mathcal{S}}$. The general structure for MM is discussed in Ref. [33], where MM is determined by a subset in \mathbb{R}^{m-1} given by the coefficients bounded by the maximum and minimum eigenvalues of the relevant left eigenmatrices L_j for $1 \leq j \leq m$.

From the perspective in temporal processing of the quantum reservoir, the higher-dimensional the MM the longer effects of the reservoir's initial states remained in the processing stream to hamper the QESP. In contrast, if the dynamics is characterized in a low-dimensional MM, the effects of the initial states are reduced faster and the local observables remain in a relaxation behavior that only depends on a finite number of history input states. This is favorable for the fading memory property of the system and enhances the performance of temporal learning tasks.

To understand the transient dynamics, we consider a specific case when the large separation occurs at $m = 2$. Here, the MM is a one-dimensional simplex, and the metastable states for this case can be considered as a linear combination of the states at end points of the MM, which are called *extreme metastable states* (EMSs) [33]. These EMSs are defined as follows:

$$\tilde{\rho}_1 = \rho_{\text{ss}} + v_2^{\text{max}} R_2, \quad \tilde{\rho}_2 = \rho_{\text{ss}} + v_2^{\text{min}} R_2, \quad (\text{S28})$$

where v_2^{max} and v_2^{min} are the maximal and minimal eigenvalues of L_2 , which are real numbers since L_2 is a Hermitian matrix. Because L_2 and ρ_{ss} are different eigenmodes of \mathcal{L} , we obtain the orthogonality as $\text{Tr}[L_2 \rho_{\text{ss}}] = 0$. From Lemma II.1 in Ref. [34] and since L_2 is a Hermitian matrix and ρ_{ss} is a Hermitian and positive semi-definite matrix, we obtain the following inequality:

$$v_2^{\text{min}} \text{Tr}[\rho_{\text{ss}}] \leq \text{Tr}[L_2 \rho_{\text{ss}}] \leq v_2^{\text{max}} \text{Tr}[\rho_{\text{ss}}]. \quad (\text{S29})$$

Because $\text{Tr}[\rho_{\text{ss}}] = 1$ and L_2 is not a zero matrix, we have $v_2^{\text{min}} \leq 0$, $v_2^{\text{max}} \geq 0$, and $v_2^{\text{max}} - v_2^{\text{min}} > 0$.

The projection of a quantum state ρ onto the MM is a linear combination of the extreme metastable states as

$$\mathcal{P}\rho = p^{(1)} \tilde{\rho}_1 + p^{(2)} \tilde{\rho}_2, \quad (\text{S30})$$

where $p^{(1,2)} = \text{Tr}[P_{1,2} \rho]$, and $P_{1,2}$ are the matrices defined by

$$P_1 = \frac{L_2 - v_2^{\text{min}} I}{\Delta v_2} \quad \text{and} \quad P_2 = \frac{-L_2 + v_2^{\text{max}} I}{\Delta v_2}, \quad (\text{S31})$$

where $\Delta v_2 = v_2^{\text{max}} - v_2^{\text{min}}$. These matrices satisfy $P_{1,2} \geq 0$ and $P_1 + P_2 = I$. Therefore $P_{1,2}$ constitute a POVM. Furthermore, the EMSs $\tilde{\rho}_1$ and $\tilde{\rho}_2$ are approximately disjoint (see Supplemental Material in Ref. [33]).

As the number of interactions $n \gg N_1$, the quantum reservoir dynamics can be captured by the effective long transient dynamics in the MM. The reservoir state corresponding with the measurement of an observable O after the n th interaction can be calculated as

$$\langle O \rangle_{\rho_n} = \sum_i p_n^{(i)} \text{Tr}[O \tilde{\rho}_i]. \quad (\text{S32})$$

In our quantum reservoir, the projection of ρ_n after the n th interaction is

$$\mathcal{P}\rho_n = p_n^{(1)}\tilde{\rho}_1 + p_n^{(2)}\tilde{\rho}_2. \quad (\text{S33})$$

We can project both the left and right side of the formula $\rho_{n+1} = \mathcal{L}(\rho_n)$ to the MM and obtain

$$p_{n+1}^{(1)}\tilde{\rho}_1 + p_{n+1}^{(2)}\tilde{\rho}_2 = p_n^{(1)}\mathcal{L}(\tilde{\rho}_1) + p_n^{(2)}\mathcal{L}(\tilde{\rho}_2). \quad (\text{S34})$$

Since λ_2 is the eigenvalue of $\tilde{\mathcal{L}}$ with the corresponding right eigenmatrix R_2 , we have

$$\begin{aligned} \mathcal{L}(\tilde{\rho}_1) &= \rho_{\text{ss}} + v_2^{\text{max}}\lambda_2 R_2 = \lambda_2\tilde{\rho}_1 + (1 - \lambda_2)\rho_{\text{ss}} \\ &= \frac{1}{\Delta v_2} \{[\lambda_2 v_2^{\text{max}} - v_2^{\text{min}}]\tilde{\rho}_1 + (1 - \lambda_2)v_2^{\text{max}}\tilde{\rho}_2\}, \end{aligned} \quad (\text{S35})$$

$$\begin{aligned} \mathcal{L}(\tilde{\rho}_2) &= \rho_{\text{ss}} + v_2^{\text{min}}\lambda_2 R_2 = \lambda_2\tilde{\rho}_2 + (1 - \lambda_2)\rho_{\text{ss}} \\ &= \frac{1}{\Delta v_2} \{(1 - \lambda_2)v_2^{\text{min}}\tilde{\rho}_1 + [v_2^{\text{max}} - \lambda_2 v_2^{\text{min}}]\tilde{\rho}_2\}. \end{aligned} \quad (\text{S36})$$

From Eqs. (S33)–(S36), the evolution dynamics on the MM can be described by the dynamics of $\mathbf{p}_n = \begin{bmatrix} p_n^{(1)} \\ p_n^{(2)} \end{bmatrix}$ as

$$\mathbf{p}_{n+1} = \frac{1}{\Delta v_2} \begin{bmatrix} \lambda_2 v_2^{\text{max}} - v_2^{\text{min}} & -(1 - \lambda_2)v_2^{\text{min}} \\ (1 - \lambda_2)v_2^{\text{max}} & v_2^{\text{max}} - \lambda_2 v_2^{\text{min}} \end{bmatrix} \mathbf{p}_n, \quad (\text{S37})$$

or

$$\Delta \mathbf{p}_n = \mathbf{p}_{n+1} - \mathbf{p}_n = A_{\text{eff}} \mathbf{p}_n, \quad (\text{S38})$$

where

$$A_{\text{eff}} = \frac{1 - \lambda_2}{\Delta v_2} \begin{bmatrix} -v_2^{\text{max}} & -v_2^{\text{min}} \\ v_2^{\text{max}} & v_2^{\text{min}} \end{bmatrix}. \quad (\text{S39})$$

Because $v_2^{\text{max}} \geq 0$ and $v_2^{\text{min}} \leq 0$ are real numbers, from Eq. (S38) we note that λ_2 must be real. Furthermore, since we assume that $|\lambda_2| < 1$, the matrix A_{eff} has non-positive diagonal terms and non-negative off-diagonal terms. The sum of entries in each column in A_{eff} is equal to 0. Therefore, A_{eff} can be considered as a generator of a discrete-time Markov chain induced from states in the MM. This generator describes the classical stochastic dynamics between two metastable states $\tilde{\rho}_1$ and $\tilde{\rho}_2$, and for $n \rightarrow \infty$ we obtain the probabilities corresponding to the stationary state ρ_{ss} .

In the numerical analysis with the model in Eq. (S25), we further investigate the eigenvalues' distribution of the reduced dynamics map \mathcal{L}_β . We first measure the ratios in absolute values between two consecutive eigenvalues as $r_k = |\lambda_{k+1}|/|\lambda_k|$, which indicate the separation of time scales in the dynamics. In Fig. S2(a), the top panel shows the expectation value of r_k over k according to the normalized time τB for 100 random \mathcal{L}_β with $N_m = 4, N_e = 2$. The bottom panel of Fig. S2(a) displays exemplary distributions of eigenvalues for $\tau B = 0.5, 1.5, 2.5, 5.0$, and 10.0. To examine the convergence property, in the top panel of Fig. S2(b), we plot the distance ratio between the trace distance of final states $\Phi_n(\rho_0^{(1)}), \Phi_n(\rho_0^{(2)})$ and the trace distance of initial states $\rho_0^{(1)}, \rho_0^{(2)}$ for the number of interaction steps going from $n = 10$ (purple line), $n = 20, 30, \dots$ to $n = 100$ (green line). This ratio is averaged over 100 different pairs of initial states maintaining $\|\rho_0^{(1)} - \rho_0^{(2)}\| > 0.5$. In the bottom panel of Fig. S2(b), the calculated ratios are displayed as the function of τB and the number n of interactions, where the color bar indicates the levels of ratios. Similarly, Fig. S2(c) indicates values of $\langle |\lambda_{k+1}|/|\lambda_k| \rangle$ as the function of J/B and α with $\tau B = 10.0$, and examples of the eigenvalues' distribution of the reduced dynamics maps \mathcal{L}_β at $\alpha = 1.0, J/B = 0.1, 0.2, 0.5, 1.0$, and 2.0.

If the eigenvalues are close to the unit border or r_k are close to 1, \mathcal{L}_β reduces toward a unitary map and the QR relaxes into a state on a high-dimensional MM. Such long transient dynamics makes the QR retain the information of its initial states on the MM. In terms of fading memory, if \mathcal{L}_β reduces toward a unitary map, then only a little information of the input state β is remained in the reservoir state after applying the reduced dynamics map \mathcal{L}_β . Therefore, the fading memory property is not enhanced in this ‘‘more unitary’’ behavior. We observe the dynamical transition ($1.5 < \tau B < 2.5$) from high values to a stable range of $\langle r_k \rangle$. In the stable range, more eigenvalues are moved near the center of the unit disk, the effects of initial states are reduced, and the dynamics will be characterized by lower-dimensional MMs in a ‘‘more ergodic’’ phase. This phase guarantees enough information in the input states to be entangled with the reservoir. The local observables then become functions of a finite number of past input states with the fading memory property. As demonstrated in the bottom panel of Fig. S2(b), the convergence property is also enhanced in this phase. We observe the similar dynamical transition in Fig. S3, where the dynamics goes from more unitary ($J/B < 0.1$) with slower relaxation to more ergodic behavior ($J/B > 0.2$) with faster relaxation.

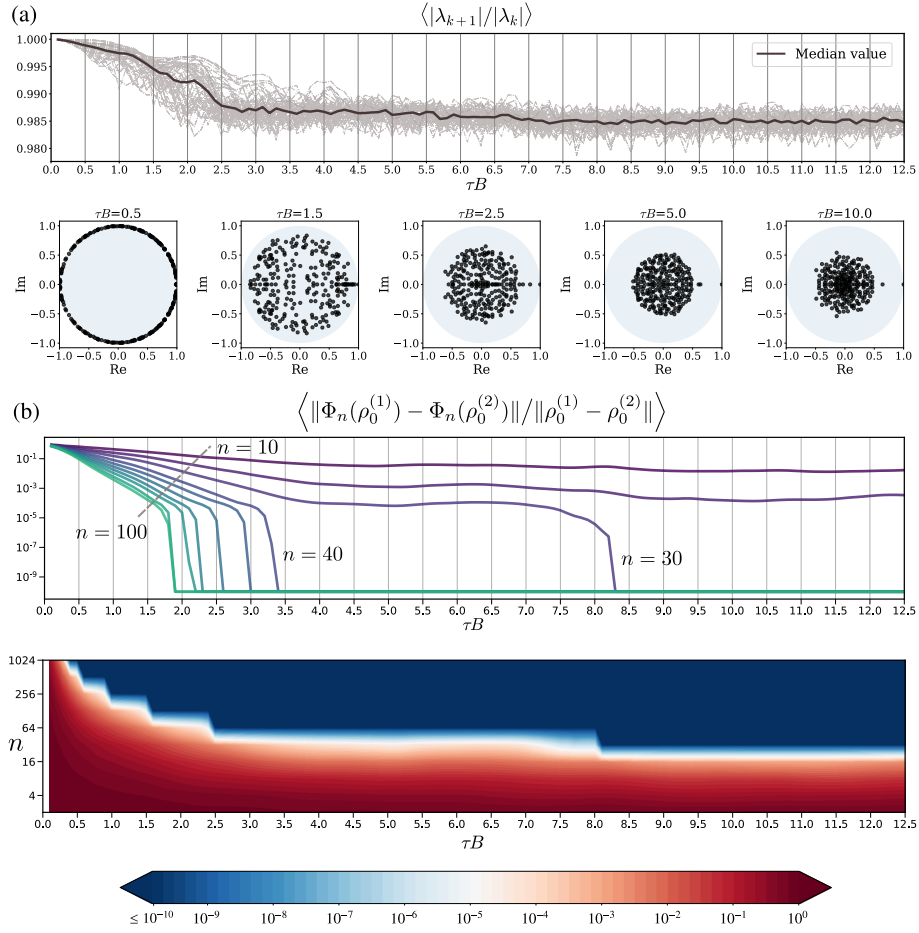


FIG. S2. (a) (Top) The values of $\langle |\lambda_{k+1}|/|\lambda_k| \rangle$ for 100 random reduced dynamics maps \mathcal{L}_β with $N_m = 4, N_e = 2, \alpha = 1.0$, and $J = B = 1.0$. The solid line depicts the median value of the ensemble of dynamics maps. (Bottom) The distribution of eigenvalues in the unit disk at $\tau B = 0.5, 1.5, 2.5, 5.0$, and 10.0 . (b) (Top) The distance ratio between the trace distance of final states $\Phi_n(\rho_0^{(1)}), \Phi_n(\rho_0^{(2)})$ and the trace distance of initial states $\rho_0^{(1)}, \rho_0^{(2)}$ for the number of interaction steps going from $n = 10$ (purple line), $n = 20, 30, \dots$ to $n = 100$ (green line). This ratio is averaged over 100 different pairs of initial states keeping $\|\rho_0^{(1)} - \rho_0^{(2)}\| > 0.5$. All values below the threshold of 10^{-10} are kept to this minimum value for clear visualization. (Bottom) The distance ratio as the function of τB and n . The levels of the ratio are indicated by the color bar.

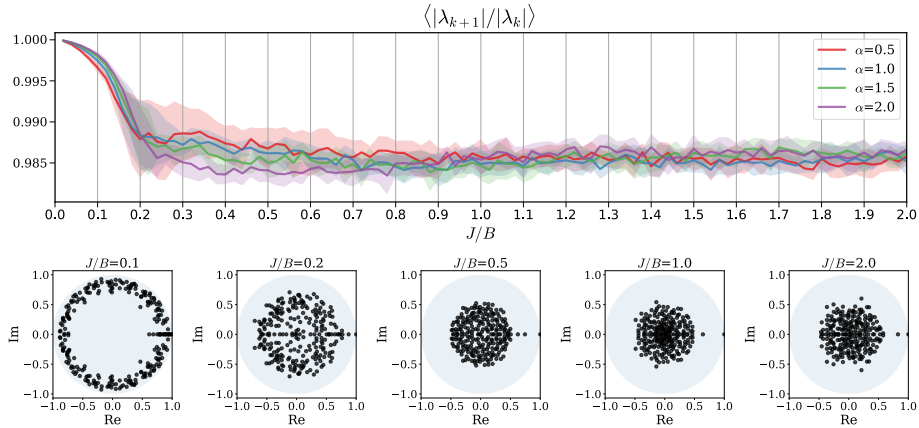


FIG. S3. (Top) Values of $\langle |\lambda_{k+1}|/|\lambda_k| \rangle$ as the function of J/B and α with $\tau B = 10.0$. The solid lines and the shaded areas indicate the median values and the confidence intervals (one standard deviation) calculated in the ensemble of 100 random \mathcal{L}_β . (Bottom) Examples of the distribution in the unit disk of eigenvalues of the reduced dynamics maps \mathcal{L}_β at $\alpha = 1.0, J/B = 0.1, 0.2, 0.5, 1.0$, and 2.0 .

IV. QUANTUM MEMORY CAPACITY

The capacity to reconstruct the previous d steps of the input states is evaluated via the square of the distance correlation [35] between the output $\{\sigma_n\}$ and the target $\{\hat{\sigma}_n\} = \{\beta_{n-d}\}$:

$$\mathcal{R}^2(d) = \frac{\mathcal{V}^2(\{\sigma_n\}, \{\hat{\sigma}_n\})}{\sqrt{\mathcal{V}^2(\{\sigma_n\}, \{\sigma_n\})\mathcal{V}^2(\{\hat{\sigma}_n\}, \{\hat{\sigma}_n\})}}. \quad (\text{S40})$$

Here, $\mathcal{V}^2(\{\rho_n\}, \{\sigma_n\})$ represents the squared distance covariance of random sequences of density matrices $\{\rho_n\}, \{\sigma_n\}$.

The squared distance covariance $\mathcal{V}^2(\{\rho_n\}, \{\sigma_n\})$ is calculated from all pairwise distances $A(\rho_j, \rho_k)$ and $A(\sigma_j, \sigma_k)$ for $j, k = 1, 2, \dots, n$. Here, the distance $A(\rho, \sigma) = \arccos F(\rho, \sigma)$ for given density matrices ρ and σ is defined as the angle induced from the fidelity $F(\rho, \sigma) = \left(\text{Tr}[\sqrt{\sqrt{\sigma}\rho\sqrt{\sigma}}]\right)^2$. We construct the distance matrices for $\{\rho_n\}$ and $\{\sigma_n\}$ as (R_{jk}) and (S_{jk}) with the elements $R_{jk} = A(\rho_j, \rho_k)$ and $S_{jk} = A(\sigma_j, \sigma_k)$. We take all double centered distances

$$r_{j,k} = R_{j,k} - \bar{R}_j - \bar{R}_k + \bar{R}_., \quad (\text{S41})$$

$$s_{j,k} = S_{j,k} - \bar{S}_j - \bar{S}_k + \bar{S}_., \quad (\text{S42})$$

where \bar{R}_j and \bar{R}_k are the j th row mean and the k th column mean, respectively, and $\bar{R}_.$ is the grand mean of the distance matrix (R_{jk}) (the same notations for S). The squared distance covariance is the arithmetic average of the products $r_{j,k}s_{j,k}$

$$\mathcal{V}^2(\{\rho_n\}, \{\sigma_n\}) = \frac{1}{n^2} \sum_{j=1}^n \sum_{k=1}^n r_{j,k}s_{j,k}. \quad (\text{S43})$$

The distance covariance and correlation are developed for measuring the dependence and testing independence between two random vectors [35]. In the definition of $\mathcal{R}^2(d)$, we are interested in the empirical distance covariance and correlation to study the serial dependence between $\{\sigma_n\}$ and $\{\hat{\sigma}_n\} = \{\beta_{n-d}\}$. Here, $0 \leq \mathcal{R}^2(d) \leq 1$, and $\mathcal{R}^2(d) = 1$ if we can find some linear transformation from the output sequence $\{\sigma_n\}$ to the target sequence $\{\hat{\sigma}_n\}$. In contrast, $\mathcal{R}^2(d) = 0$ implies that the system cannot reconstruct the previous d steps of the inputs because the output and the target sequences are completely independent. We define $\mathcal{R}^2(d)$ as the *quantum memory function* of the quantum reservoir to represent the fraction of distance variance explainable in a sequence of states by other. We then define the *quantum memory capacity* as $\text{QMC} = \sum_{d=0}^{\infty} \mathcal{R}^2(d)$ to measure how much distance variance of the delay input states can be recovered from reconstructed output states, summed over all delays.

QMC is motivated from the memory capacity in classical reservoir computing [36] and is generally proposed here as a standard quantity to compare the temporal processing capacity of quantum devices. We note that without the condition of the quantum states, σ_n and $\hat{\sigma}_n$ can be written in the vector form, and QMC can be defined in a same way with the classical memory capacity in Ref. [1] and Definition 1 in Ref. [37]. In this situation, QMC is bounded by the number of elements (MK) in each reservoir state if the input states are i.i.d. We hypothesize that this bound is still true for the definition of $\mathcal{R}^2(d)$ and QMC in our framework.

Figure S4 shows QMC as a function of τB broken down in values of d ($0 \leq d \leq 7$) with the model parameters $\alpha = 1.0, J = 1.0, J/B = 1.0$, and $N_e = 2, N_m = 4$. Here, the number of observables is set to $K = N_m$ if we only select the observables as spin projections $O_j = \hat{s}_j^z$ for all j , and to $K = N_m(N_m + 1)/2$ if we further select the observables as two-spins correlations $\hat{s}_i^z \hat{s}_j^z$ for all $i < j$. The first 1000 time steps are excluded for initial transients to satisfy the QESP. The training and evaluating are performed with 3000 and 1000 time steps, respectively. The value of $\mathcal{R}^2(d)$ is averaged over different runs with ten random trials of the initial state and input sequence. This value is faded out as increasing the delay $d \geq 7$. This value is increased as increasing the measurement multiplexity (M) and the number of observables (K) to obtain high fidelities in tomography tasks. We note that increasing M may be more realistic since it appears difficult to find many physical quantities that can be measured in the physical implementation. However, related to the quantum Zeno effect [38], we should not set the value $\tau B/M$ as too small, since in this case, the time evolution slows down and the frequent measurements force the quantum state to remain in a projected subspace.

We plot other numerical results for QMC in Figs. S5–S8. In these numerical simulations, the first 1000 time steps are excluded for initial transients to satisfy the QESP. The training and evaluating are performed with 3000 and 100 time steps, respectively. The capacity is averaged over ten random trials of input sequences and initial states.

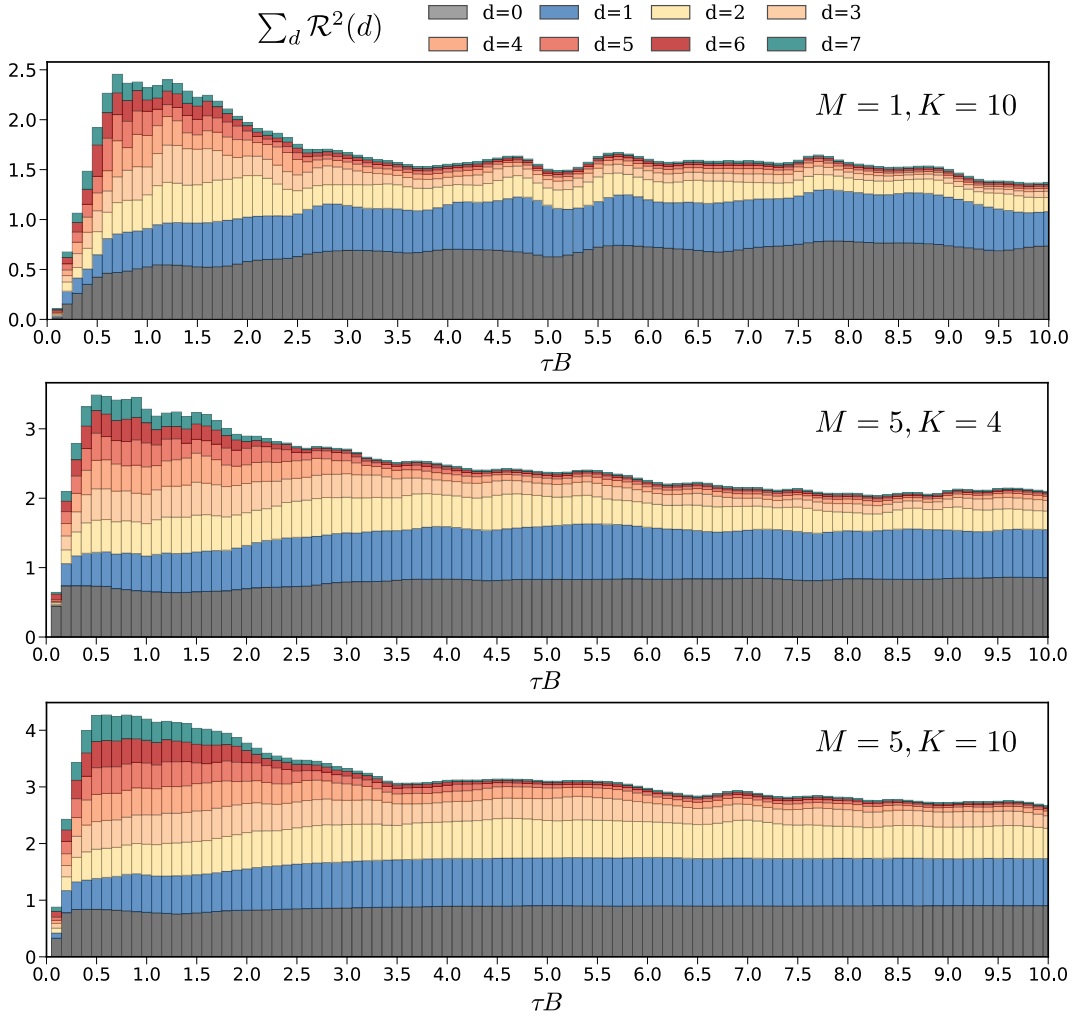


FIG. S4. The quantum memory capacity $\sum_d \mathcal{R}^2(d)$ broken down in different d ($0 \leq d \leq 7$) according to τB with $\alpha = 1.0$, $J = 1.0$, $J/B = 1.0$, $N_e = 2$, $N_m = 4$, and different values of measurement multiplexity M and number K of observables.

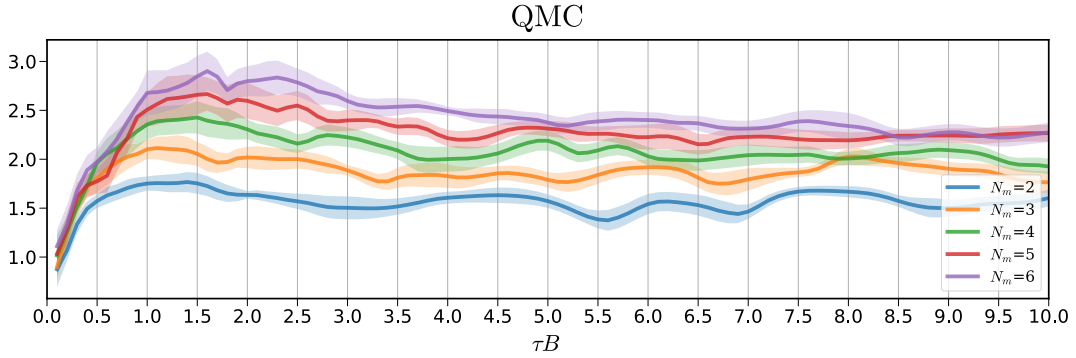


FIG. S5. Quantum memory capacity (QMC) for sequences of i.i.d. two-qubit states of the quantum reservoir modeled in Eq. (S25) according to the normalized interaction time τB and the number N_m of qubits in the reservoir. Other model parameters are $\alpha = 1.0$, $J = 1.0$, and $J/B = 1.0$. QMC is calculated until $d_{\max} = 20$. The lines depict the average QMC across 10 sequences of i.i.d. input states. The shaded areas indicate the confidence intervals (one standard deviation) calculated in the same ensemble of runs.

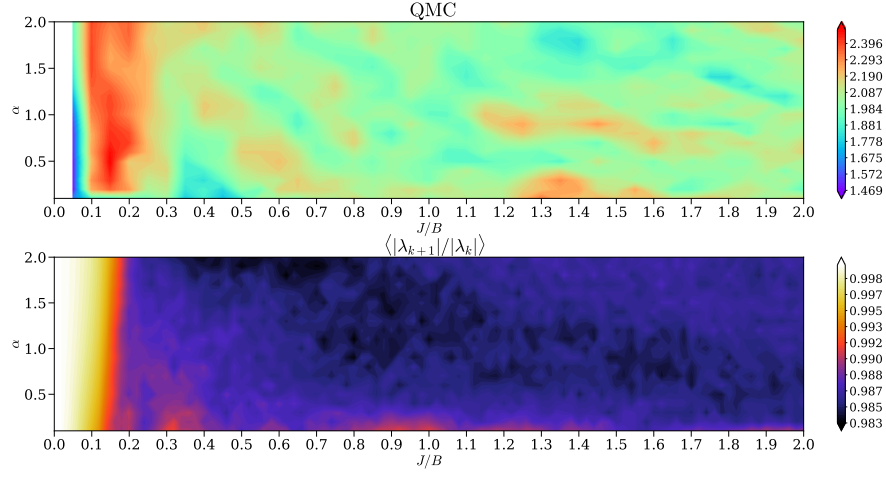


FIG. S6. (Top) Quantum memory capacity (calculated until $d_{\max} = 10$) as the function of model parameters α and J/B with $N_e = 2, N_m = 4$, and $\tau B = 10.0$. (Bottom) The value $\langle |\lambda_{k+1}|/|\lambda_k| \rangle$ over k as the function of model parameters.

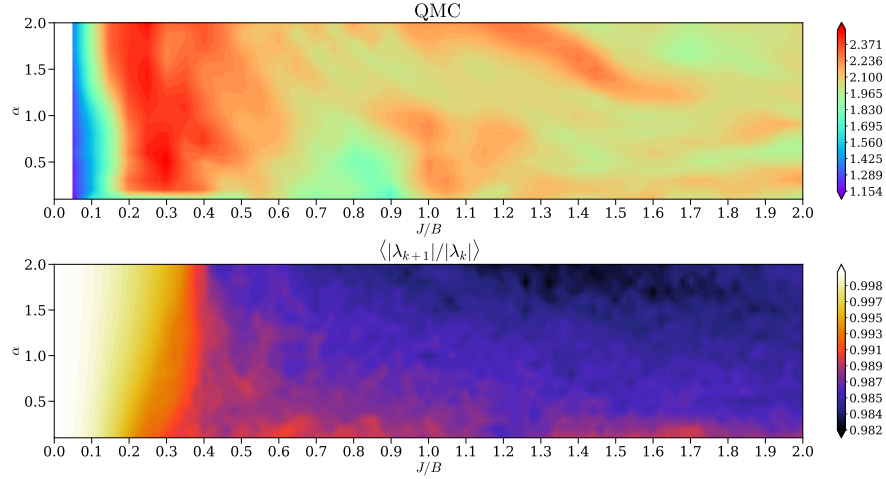


FIG. S7. (Top) Quantum memory capacity (calculated until $d_{\max} = 10$) as the function of model parameters α and J/B with $N_e = 2, N_m = 4$, and $\tau B = 5.0$. (Bottom) The value $\langle |\lambda_{k+1}|/|\lambda_k| \rangle$ over k as the function of model parameters.

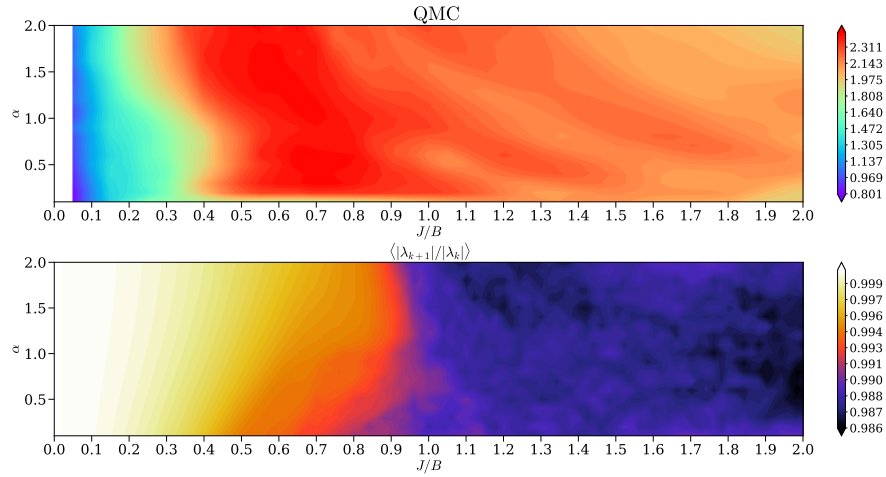


FIG. S8. (Top) Quantum memory capacity (calculated until $d_{\max} = 10$) as the function of model parameters α and J/B with $N_e = 2, N_m = 4$, and $\tau B = 2.0$. (Bottom) The value $\langle |\lambda_{k+1}|/|\lambda_k| \rangle$ over k as the function of model parameters.

V. RESULTS ON THE TEMPORAL TOMOGRAPHY TASKS

Given a sequence of input states β_1, β_2, \dots in a Hilbert space \mathcal{H}_A with the dimension D_A , we consider the temporal map \mathcal{F} as

$$\mathcal{F}(\beta_n) = \frac{1}{Z} \sum_{i=0}^d \eta_i \Omega_{n-i}(\beta_{n-i}), \quad (\text{S44})$$

where $\Omega_1, \Omega_2, \dots$ is a sequence of unknown quantum channels from \mathcal{H}_A to another Hilbert space, and $\eta_0, \eta_1, \dots, \eta_d$ are unknown non-negative real numbers with $Z = \sum_{i=0}^d \eta_i$ to preserve the trace. Our objective is to characterize \mathcal{F} from the measurement data. If $\eta_i = 1$ for all i , we can consider \mathcal{F} as a quantum version of the simple moving average filter for a sequence of quantum channels $\Omega_1, \Omega_2, \dots$ acting on the input states. If $\eta_i = (d+1-i)$ for all i , we have a weighted moving average filter. If $\eta_d = 1$ and $\eta_i = 0$ for $i \neq d$, we have a memory-based reconstruction of the channel applied on d -delay quantum states. In our demonstration, we set Ω_n as a time-dependent depolarizing quantum channel $\Omega_n(\beta) = p_n \frac{I}{D} + (1-p_n)\beta$. The depolarizing probability p_n is formulated as the r th-order nonlinear dynamical output $p_n = \kappa p_{n-1} + \eta p_{n-1} \left(\sum_{j=0}^{r-1} p_{n-j-1} \right) + \gamma u_{n-r+1} u_n + \delta$, where $r = 10, \kappa = 0.3, \eta = 0.04, \gamma = 1.5$, and $\delta = 0.1$. Here, $\{u_n\}$ is a random sequence of scalar values in $[0, 0.2]$ to set p_n into the stable range in $[0, 1]$. The sequence $\{p_n\}$ resembles the NARMA benchmark [39], which is commonly used for evaluating the computational capability of temporal processing with long time dependence. Furthermore, the sequence $\{u_n\}$ is randomly generated with the same random seed used for generating the input sequence $\{\beta_n\}$; therefore, $\{p_n\}$ depends on $\{\beta_n\}$. This setting makes the quantum channel Ω_n dependent on to the current input and the output of previous channels, then the tomography task requires memory to characterize these channels.

Figure S9 illustrates an example of a memory-based reconstruction of the delayed depolarizing quantum map ($\eta_d = 1$ and $\eta_i = 0$ for $i \neq d$) with delay time $d = 5, N_m = 5, N_e = 1$, and the measurement multiplexity $M = 1, 5$. Other model parameters are $\alpha = 1.0, J/B = 1.0$. Here, the first $t_{\text{buffer}} = 500$ time steps are excluded for initial transients to satisfy the QESP. The training and evaluating are performed in the range $(t_{\text{buffer}}, t_{\text{train}}]$ and $(t_{\text{train}}, t_{\text{val}}]$, respectively, where $t_{\text{train}} = 1000$ and $t_{\text{val}} = 1200$. At each time point, the $D \times D$ density matrix is represented as a vector with $2D^2$ elements by stacking the real and imaginary parts. The plots with a green-yellow color map in Fig. S9 show the absolute error between the target and the predicted vector at $M = 1$ and $M = 5$. The red points in these plots indicate the fidelities between the target and the predicted quantum states. We confirm that we can nearly reconstruct the previous depolarizing quantum channel almost perfectly as the fidelities are above 95% (with $M = 5$).

Figure S10 illustrates an example of a simple moving average filter ($\eta_i = 1$ for all i) for a sequence of quantum channels $\Omega_1, \Omega_2, \dots$ acting on the input states with the delay time $d = 5, N_m = 5, N_e = 1$, and the measurement multiplexity $M = 1, 5$. Other parameters are $\alpha = 1.0, J/B = 1.0, t_{\text{buffer}} = 500, t_{\text{train}} = 1000$, and $t_{\text{val}} = 1200$. Here, the input states jump to a new random quantum state every 20 time steps, thus introducing temporal dependencies between input states. Our framework can reconstruct this intriguing tomography of a simple moving average filter.

Figure S11 and Fig. S12 illustrate the other results for the tomography task $F(\beta_n) = \Omega_{n-1}(\beta_{n-1})$ demonstrated in the main text. The first $t_{\text{buffer}} = 1000$ time steps are excluded for initial transients to satisfy the QESP, the training and evaluating are performed in the range $(t_{\text{buffer}}, t_{\text{train}}]$ and $(t_{\text{train}}, t_{\text{val}}]$, respectively, where $t_{\text{train}} = 4000$ and $t_{\text{val}} = 5000$. Other model parameters are $\alpha = 1.0, J/B = 1.0$. Figure S11 illustrates the calculated RMSF as functions of N_m, N_e , and τB with the measurement multiplexity $M = 1, 5$, and the number of observables is $K = N_m$. The RMSF is averaged over ten different runs with random trials of the input sequence and initial state. We confirm that increasing N_m and M indeed scales the fidelity.

Figure S12(a) illustrates the calculated error (1.0 - RMSF) as functions of τB with the measurement multiplexity $M = 5$ for different values of N_e, N_m and K . Here, the number of observables is set to $K = N_m$ if we only select the observables as spin projections $O_j = \hat{s}_j^z$ for all j , and to $K = N_m(N_m + 1)/2$ if we further select the observables as two-spins correlations $\hat{s}_i^z \hat{s}_j^z$ for all $i < j$. The error is averaged over ten different runs with random trials of the input sequence and initial state. The fidelity is larger than 94% even with $N_e = 3$ qubits and $N_m = 4, 5$.

We further compare our method with the classical baseline method, which uses linear regression for the sequence of input density matrices to obtain the sequence of output density matrices. Therefore, this baseline method does not have memory effect to emulate the recurrent relation in the temporal quantum map. In the classical baseline method, we assume that we can obtain full tomography of input states, which is not required in our method. Instead of using the measurement results in the quantum reservoir, reservoir state \mathbf{x}_n is constructed directly from the vector form of β_n by stacking the real and imaginary parts in the corresponding density matrix. The readout map and training process are the same as our method. In Fig. S12(b), we compare our method with the baseline method in terms of tomography error (1.0 - RMSF) for the reconstruction task of $\mathcal{F}(\beta_n) = \Omega_{n-1}(\beta_{n-1})$ for different values of N_e, N_m , and K . We confirm that our method with short-term memory property outperforms the baseline method for

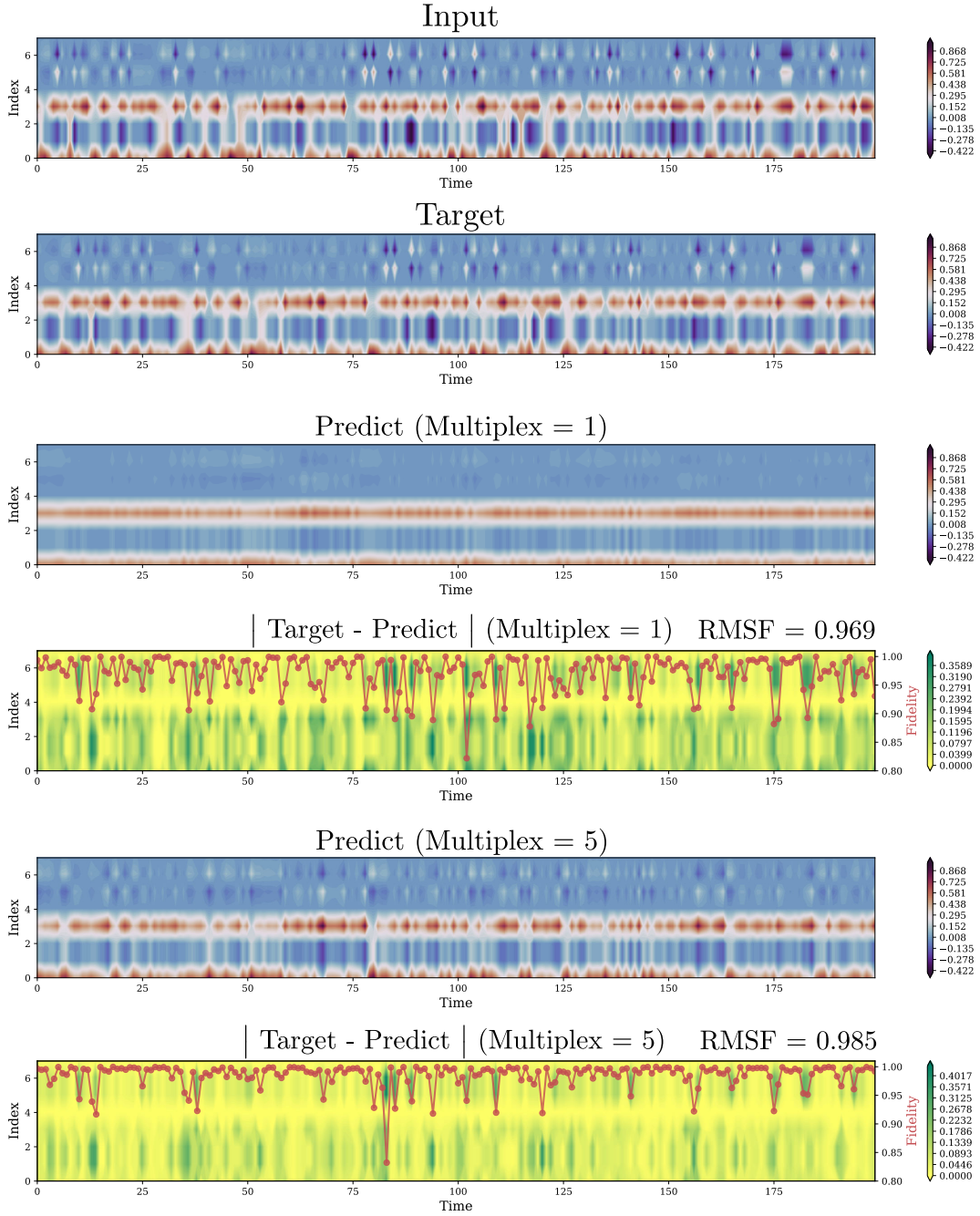


FIG. S9. Contour plots of a temporal forecast with the absolute difference between the target and the prediction for the reconstruction of delayed depolarizing quantum map with delay time $d = 5$, $N_m = 5$, and $N_e = 1$. Other model parameters are $\alpha = 1.0$, $J = 1.0$, $J/B = 1.0$, and $\tau B = 2.0$. At each time point, the 2×2 density matrix is represented as a vector with 8 elements by stacking the real and imaginary parts. The red points in the plots with green-yellow color maps (with right y-axis) represent the fidelities at each time point between the target and the predicted state.

all settings of N_e , N_m , and K . We note that our method does not need to perform full tomography for input states as the baseline method but rather perform measurements with a single and controllable setup for a quantum reservoir to obtain the reservoir states to train the recurrent relation in the temporal quantum map.

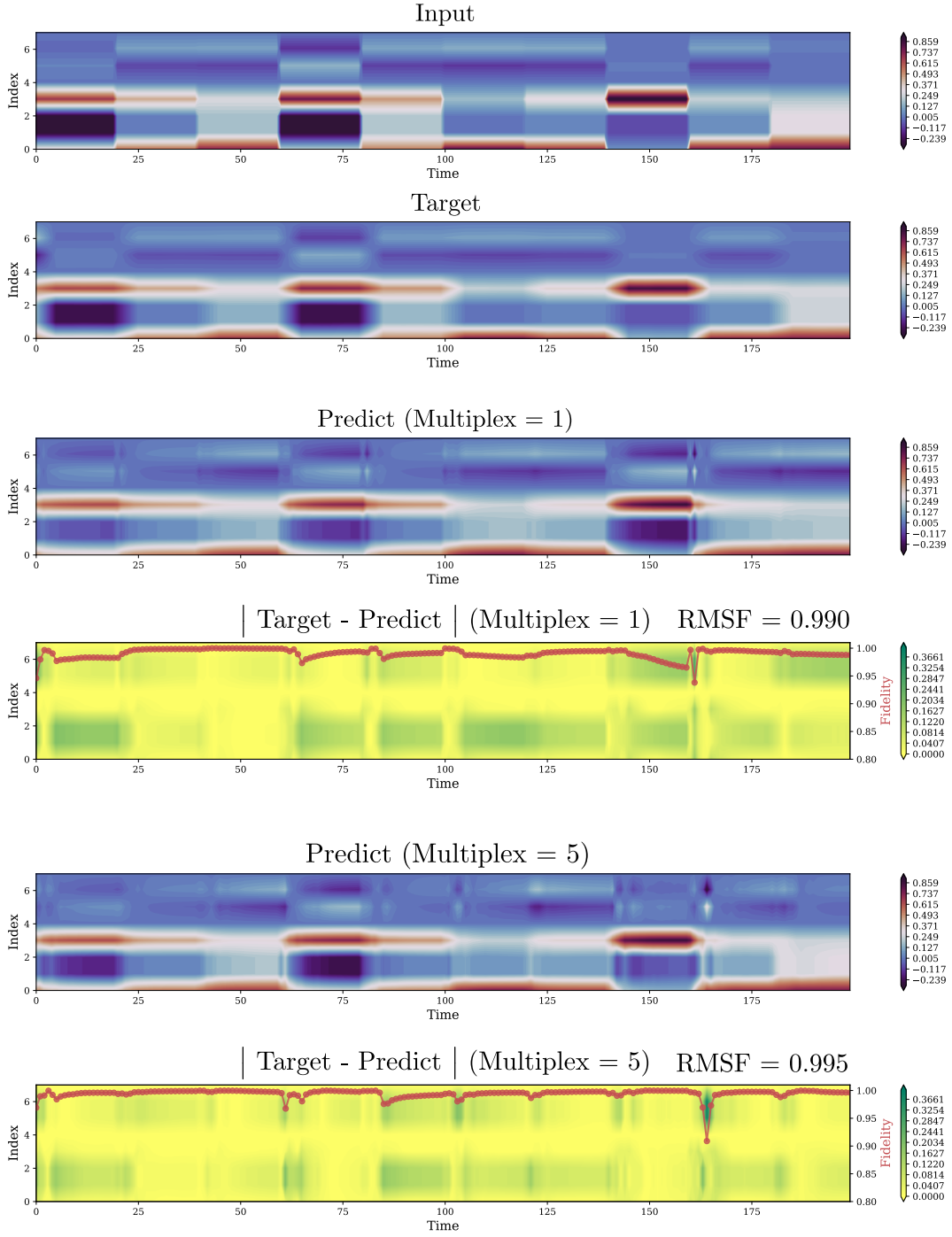


FIG. S10. Contour plots of a temporal forecast with the absolute difference between the target and the prediction for the reconstruction of a simple moving average filter for a sequence of depolarizing quantum channels with delay time $d = 5$, $N_m = 5$, and $N_e = 1$. Other model parameters are $\alpha = 1.0$, $J = 1.0$, $J/B = 1.0$, and $\tau B = 2.6$. At each time point, the 2×2 density matrix is represented as a vector with 8 elements by stacking the real and imaginary parts. The red points in the plots with green-yellow color maps (with right y-axis) represent the fidelities at each time point between the target and the predicted state. Here, the input states jump to a new random quantum state every 20 time steps, thus introducing temporal dependencies between input states.

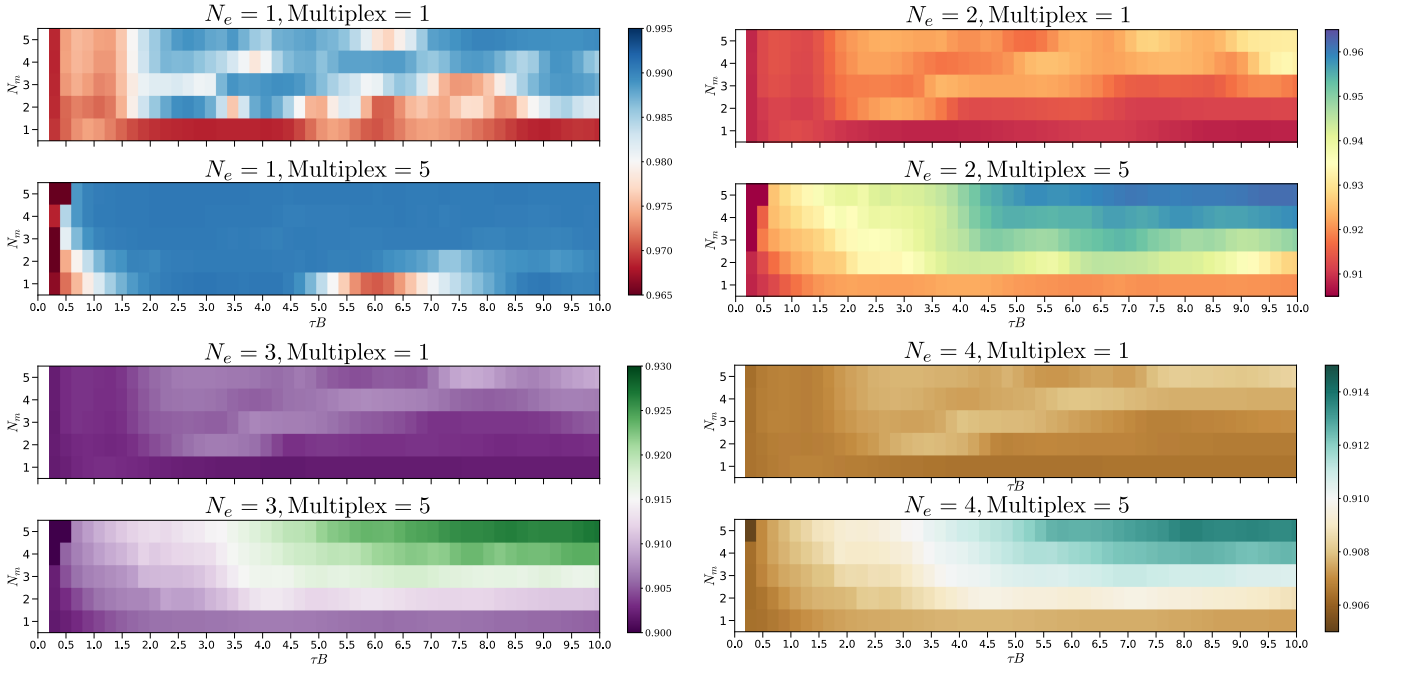


FIG. S11. Fidelities as functions of N_m , N_e , and the normalized interaction time τB for the memory-based reconstruction of delayed depolarizing quantum map $\mathcal{F}(\beta_n) = \Omega_{n-d}(\beta_{n-d})$ with delay $d = 1$. The levels of fidelity values are indicated by the color bars.

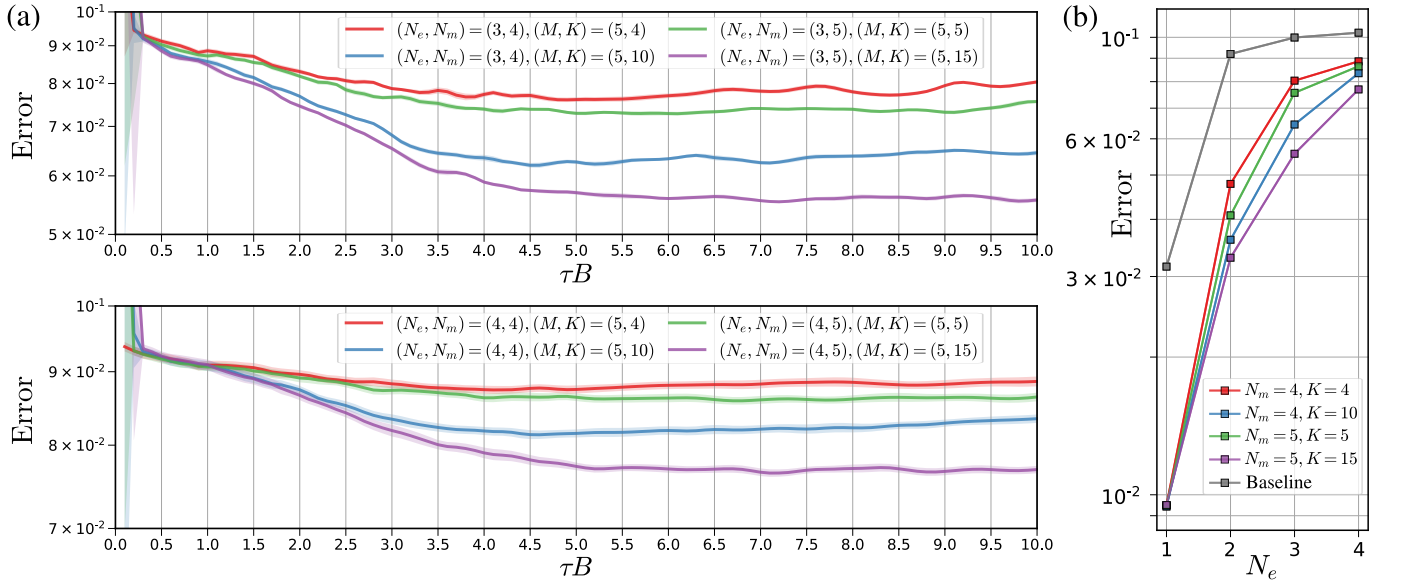


FIG. S12. (a) Tomography errors ($1.0 - \text{RMSF}$) for input states of $N_e = 3, 4$ qubits and the quantum reservoir of $N_m = 4, 5$ qubits as functions of τB for the reconstruction of delayed depolarizing quantum map $\mathcal{F}(\beta_n) = \Omega_{n-d}(\beta_{n-d})$ with $d = 1$. Other model parameters are $\alpha = 1.0$, $J/B = 1.0$. (b) Tomography errors of the baseline and our method for different N_e , N_m , and K at $\tau B = 10.0$.

-
- [1] H. Jaeger, The “echo state” approach to analysing and training recurrent neural networks—with an erratum note, [Bonn, Germany: German National Research Center for Information Technology GMD Technical Report 148](#), 13 (2001).
- [2] W. Maass, T. Natschläger, and H. Markram, Real-time computing without stable states: A new framework for neural computation based on perturbations, [Neural Computation 14](#), 2531 (2002).
- [3] M. Lukoševičius and H. Jaeger, Reservoir computing approaches to recurrent neural network training, [Comput. Sci. Rev. 3](#), 127 (2009).
- [4] K. Nakajima, Physical reservoir computing—an introductory perspective, [Jpn. J. Appl. Phys. 59](#), 060501 (2020).
- [5] K. Fujii and K. Nakajima, Harnessing disordered-ensemble quantum dynamics for machine learning, [Phys. Rev. Applied 8](#), 024030 (2017).
- [6] K. Nakajima, K. Fujii, M. Negoro, K. Mitarai, and M. Kitagawa, Boosting computational power through spatial multiplexing in quantum reservoir computing, [Phys. Rev. Applied 11](#), 034021 (2019).
- [7] S. Ghosh, A. Opala, M. Matuszewski, T. Paterek, and T. C. Liew, Quantum reservoir processing, [npj Quantum Inf. 5](#), 1 (2019).
- [8] S. Ghosh, A. Opala, M. Matuszewski, T. Paterek, and T. C. H. Liew, Reconstructing quantum states with quantum reservoir networks, [IEEE Trans. Neural Netw. Learn. Syst. 32](#), 3148 (2020).
- [9] S. Ghosh, T. Paterek, and T. C. H. Liew, Quantum neuromorphic platform for quantum state preparation, [Phys. Rev. Lett. 123](#), 260404 (2019).
- [10] J. Nokkala, R. Martínez-Peña, G. L. Giorgi, V. Parigi, M. C. Soriano, and R. Zambrini, Gaussian states of continuous-variable quantum systems provide universal and versatile reservoir computing, [Commun. Phys. 4](#), 53 (2021).
- [11] L. C. G. Góvia, G. J. Ribeill, G. E. Rowlands, H. K. Krovi, and T. A. Ohki, Quantum reservoir computing with a single nonlinear oscillator, [Preprint at arXiv:2004.14965](#) (2020).
- [12] M. Negoro, K. Mitarai, K. Nakajima, and K. Fujii, Toward NMR quantum reservoir computing, in [Reservoir Computing: Theory, Physical Implementations, and Applications](#), edited by K. Nakajima and I. Fischer (Springer Singapore, Singapore, 2021) pp. 451–458.
- [13] J. Chen, H. I. Nurdin, and N. Yamamoto, Temporal information processing on noisy quantum computers, [Phys. Rev. Applied 14](#), 024065 (2020).
- [14] S. Dasgupta, K. E. Hamilton, and A. Banerjee, Designing a NISQ reservoir with maximal memory capacity for volatility forecasting, [Preprint at arXiv:2004.08240](#) (2020).
- [15] D. S. Abrams and S. Lloyd, Quantum algorithm providing exponential speed increase for finding eigenvalues and eigenvectors, [Phys. Rev. Lett. 83](#), 5162 (1999).
- [16] M. A. Nielsen and I. L. Chuang, [Quantum Computation and Quantum Information: 10th Anniversary Edition](#), 10th ed. (Cambridge University Press, USA, 2011).
- [17] M. Mohseni, A. T. Rezakhani, and D. A. Lidar, Quantum-process tomography: Resource analysis of different strategies, [Phys. Rev. A 77](#), 032322 (2008).
- [18] Y. Chen and X. Ye, Projection onto a simplex, [Preprint at arXiv:1101.6081](#) (2011).
- [19] B. I. Bantysh, A. Y. Chernyavskiy, and Y. I. Bogdanov, Quantum tomography benchmarking, [Preprint at arXiv:2012.15656](#) (2020).
- [20] Y. Quek, S. Fort, and H. K. Ng, Adaptive quantum state tomography with neural networks, [npj Quantum Inf. 7](#), 105 (2021).
- [21] S. Boyd and L. Chua, Fading memory and the problem of approximating nonlinear operators with volterra series, [IEEE Trans. Circuits Syst. 32](#), 1150 (1985).
- [22] Q. H. Tran and K. Nakajima, Higher-order quantum reservoir computing, [Preprint at arXiv:2006.08999](#) (2020).
- [23] J. Chen and H. I. Nurdin, Learning nonlinear input–output maps with dissipative quantum systems, [Quantum Inf. Process. 18](#), 198 (2019).
- [24] L. Bruneau, A. Joye, and M. Merkli, Infinite products of random matrices and repeated interaction dynamics, [Ann. Inst. H. Poincaré Probab. Statist. 46](#), 442 (2010).
- [25] I. Nechita and C. Pellegrini, Random repeated quantum interactions and random invariant states, [Probab. Theory Relat. Fields 152](#), 299 (2010).
- [26] R. Movassagh and J. Schenker, An ergodic theorem for homogeneously distributed quantum channels with applications to matrix product states, [Preprint at arXiv:1909.11769](#) (2019).
- [27] R. Movassagh and J. Schenker, Theory of ergodic quantum processes, [Preprint at arXiv:2004.14397](#) (2020).
- [28] J. M. Steele, Kingman’s subadditive ergodic theorem, [Ann. Inst. H. Poincaré Probab. Statist. 25](#), 93 (1989).
- [29] H. Hennion, Limit theorems for products of positive random matrices, [Ann. Probab. 25](#), 1545 (1997).
- [30] D. Porras and J. I. Cirac, Effective quantum spin systems with trapped ions, [Phys. Rev. Lett. 92](#), 207901 (2004).
- [31] K. Kim, M.-S. Chang, R. Islam, S. Korenblit, L.-M. Duan, and C. Monroe, Entanglement and tunable spin-spin couplings between trapped ions using multiple transverse modes, [Phys. Rev. Lett. 103](#), 120502 (2009).
- [32] P. Jurcevic, B. P. Lanyon, P. Hauke, C. Hempel, P. Zoller, R. Blatt, and C. F. Roos, Quasiparticle engineering and entanglement propagation in a quantum many-body system, [Nature 511](#), 202 (2014).
- [33] K. Macieszczak, M. Guță, I. Lesanovsky, and J. P. Garrahan, Towards a theory of metastability in open quantum dynamics, [Phys. Rev. Lett. 116](#), 240404 (2016).
- [34] J. B. Lasserre, A trace inequality for matrix product, [IEEE Trans. Autom. Control. 40](#), 1500 (1995).

- [35] G. J. Székely, M. L. Rizzo, and N. K. Bakirov, Measuring and testing dependence by correlation of distances, [Ann. Stat.](#) **35**, 2769 (2007).
- [36] H. Jaeger, Short term memory in echo state networks (GMD-Forschungszentrum Informationstechnik, 2001) p. 60.
- [37] J. Dambre, D. Verstraeten, B. Schrauwen, and S. Massar, Information processing capacity of dynamical systems, [Sci. Rep.](#) **2**, 514 (2012).
- [38] B. Misra and E. C. G. Sudarshan, The Zeno's paradox in quantum theory, [J. Math. Phys.](#) **18**, 756 (1977).
- [39] A. Atiya and A. Parlos, New results on recurrent network training: unifying the algorithms and accelerating convergence, [IEEE Trans. Neural Netw. Learn. Syst.](#) **11**, 697 (2000).